JOURNAL OF PETROLOGY | VOLUME 54 | NUMBER 2 | PAGES 235–271 | 2013 | doi:10.1093/petrology/egs068

On the Time Scales of Magma Genesis, Melt Evolution, Crystal Growth Rates and Magma Degassing in the Erebus Volcano Magmatic System Using the ^{238}U, ^{235}U and ^{232}Th Decay Series

KENNETH W. W. SIMS[1,2]*, SYLVAIN PICHAT[3], MARK K. REAGAN[4], PHILIP R. KYLE[5], HENRIETTA DULAIOVA[2,6], NELIA W. DUNBAR[7], JULIE PRYTULAK[8,9], GEORGINA SAWYER[10], GRAHAM D. LAYNE[2,11], JANNE BLICHERT-TOFT[3], PIERRE J. GAUTHIER[12], MATTHEW A. CHARETTE[2] AND TIMOTHY R. ELLIOTT[8]

[1]WYOMING HIGH-PRECISION ISOTOPE LABORATORY, DEPARTMENT OF GEOLOGY AND GEOPHYSICS, UNIVERSITY OF WYOMING, LARAMIE, WY 82070, USA

[2]WOODS HOLE OCEANOGRAPHIC INSTITUTION, WOODS HOLE, MA 02543, USA

[3]LABORATOIRE DE GEOLOGIE DE LYON, CNRS UMR 5276, ECOLE NORMALE SUPERIEURE DE LYON, 46, ALLEE D'ITALIE 69364 LYON CEDEX 7, FRANCE

[4]DEPARTMENT OF GEOSCIENCES, UNIVERSITY OF IOWA, IOWA CITY, IA 52242, USA

[5]DEPARTMENT OF EARTH AND ENVIRONMENTAL SCIENCES, NEW MEXICO INSTITUTE OF MINING AND TECHNOLOGY, SOCORRO, NM 87801, USA

[6]DEPARTMENT OF GEOLOGY AND GEOPHYSICS, UNIVERSITY OF HAWAI'I AT MANOA, HONOLULU, HI 96822, USA

[7]NEW MEXICO BUREAU OF GEOLOGY AND MINERAL RESOURCES, NEW MEXICO INSTITUTE OF MINING AND TECHNOLOGY, SOCORRO, NM 87801, USA

[8]BRISTOL ISOTOPE GROUP, SCHOOL OF EARTH SCIENCES, UNIVERSITY OF BRISTOL, BRISTOL, BS8 1RJ, UK

[9]DEPARTMENT OF EARTH SCIENCE AND ENGINEERING, IMPERIAL COLLEGE, LONDON, SW7 2AZ, UK

[10]DEPARTMENT OF GEOGRAPHY, UNIVERSITY OF CAMBRIDGE, DOWNING PLACE, CAMBRIDGE CB2 3EN, UK

[11]DEPARTMENT OF EARTH SCIENCES, MEMORIAL UNIVERSITY OF NEWFOUNDLAND, ST. JOHN'S, NL A1B 3X5, CANADA

[12]LABORATOIRE MAGMAS ET VOLCANS, CNRS, CLERMONT-FERRAND 63000, FRANCE

RECEIVED MARCH 25, 2012; ACCEPTED SEPTEMBER 4, 2012
ADVANCE ACCESS PUBLICATION OCTOBER 13, 2012

We investigate the time scales of magma genesis, melt evolution, crystal growth rates and magma degassing in the Erebus volcano magmatic system using measurements of ^{238}U–^{230}Th–^{226}Ra–^{210}Pb–^{210}Po, ^{232}Th–^{228}Ra–^{228}Th and ^{235}U–^{231}Pa–^{227}Ac. These are the first measurements of ^{231}Pa–^{227}Ac in volcanic samples and represent the first set of data in a volcanic system to examine the entire suite of

*Corresponding author. Present address: Wyoming High-Precision Isotope Laboratory, Department of Geology and Geophysics, University of Wyoming, Laramie, WY 82070, USA. E-mail: ksims7@uwyo.edu

relevant ^{238}U, ^{235}U and ^{232}Th decay series nuclides. Our sample suite consists of 22 phonolite volcanic bombs, erupted between 1972 and 2005, and five anorthoclase megacrysts separated from bombs erupted in 1984, 1989, 1993, 2004 and 2005. The ^{238}U–^{230}Th, ^{230}Th–^{226}Ra and ^{235}U–^{231}Pa systems are uniform over the 34 years examined. The anorthoclase megacrysts and phonolite glasses show complementary $^{226}Ra/^{230}Th$ disequilibria with ($^{226}Ra/^{230}Th$) ~40 in the anorthoclase and ~0·75 in the phonolite glass. In all samples, ($^{210}Pb/^{226}Ra$) is in radioactive equilibrium for both phases. In two phonolite glass samples ($^{227}Ac/^{231}Pa$) is unity. For the phonolite glasses ($^{228}Ra/^{232}Th$) is in equilibrium, whereas in the anorthoclase megacrysts it is significantly greater than unity. Instantaneous crystal fractionation, with magma residence times greater than 100 years and less than 10 kyr, can account for the measured ^{238}U–^{230}Th–^{226}Ra–^{210}Pb and ^{235}U–^{231}Pa–^{227}Ac. However, the significant $^{228}Ra/^{232}Th$ disequilibria in the anorthoclase megacrysts preclude this simple interpretation. To account for this apparent discrepancy we therefore developed an open-system, continuous crystallization model that incorporates both nuclide ingrowth and decay during crystallization. This open-system model successfully reproduces all of the measured ^{238}U and ^{232}Th disequilibria and suggests that the shallow magma reservoir at Erebus is growing. The implication of this modeling is that when the time scale of crystallization is comparable with the half-life of the daughter nuclide of interest (e.g. ^{226}Ra) the simple isochron techniques typically used in most U-series studies can provide erroneous ages. The observation that ($^{210}Pb/^{226}Ra$) and ($^{227}Ac/^{231}Pa$) are in radioactive equilibrium suggests that the residence time of the magmas is >100 years. When considering the effect of ^{222}Rn degassing on $^{210}Pb/^{226}Ra$, the data indicate that the majority of magma degassing is deep and long before eruption, consistent with melt inclusion data. Additionally, for the 2005 lava bomb, whose eruption date (16 December 2005) is known explicitly, ^{210}Po was not completely degassed from the magma at the time of eruption. Incomplete degassing of ^{210}Po is atypical for subaerially erupted lavas and suggests that the Erebus shallow magma degasses about 1% of its Po per day. The combined ^{238}U and ^{232}Th data further indicate that the pyroclasts ejected by Strombolian eruptions at Erebus have compositions that are close to what would be expected for a near-steady-state system, reflecting inmixing of degassed magmas, crystal fractionation, and aging.

KEY WORDS: *Erebus volcano; U-series isotopes; HIMU; Antarctica; magma chamber residence time; open-system crystallization; magma degassing*

INTRODUCTION

The persistent lava lake at Erebus volcano, Antarctica, provides an unparalleled opportunity to study the time scales and rates of crystallization and magma degassing in an active alkaline magmatic system. Determining these time scales is fundamental to our physical understanding of eruption dynamics and critical for hazard assessment.

The Erebus lava lake is the top of a convecting magma conduit, which is continuously and quiescently degassing. Infrequent Strombolian eruptions often eject phonolite bombs onto the crater rim where they can be sampled. These bombs have provided an almost annual record of the magma composition from the early 1970s to the present. The highly evolved phonolite magma contains ~30% anorthoclase megacrysts reaching up to 10 cm in length, which makes it a rarity among alkaline systems. A wealth of observational, geophysical, petrological and geochemical data provides a comprehensive and detailed perspective of the genesis and evolution of the Erebus volcanic system and the dynamics of the current lava lake (Giggenbach *et al.*, 1973; Kyle & Cole, 1974; Kyle *et al.*, 1982, 1992; Kyle, 1990*a*, 1990*b*; Reagan *et al.*, 1992; Dunbar *et al.*, 1994; Zreda-Gostynska *et al.*, 1997; Esser *et al.*, 2004; Harpel *et al.*, 2004; Sims & Hart, 2006; Oppenheimer & Kyle, 2008, and papers therein; Oppenheimer *et al.*, 2011).

The magmatic evolution of the Erebus lavas has been studied extensively and is convincingly interpreted in terms of simple magma differentiation processes (Kyle *et al.*, 1992). In this contribution, we investigate the time scales of magma genesis, melt evolution, crystal growth rates and magma degassing in the Erebus magmatic system using measurements of ^{238}U–^{230}Th–^{226}Ra–^{210}Pb–^{210}Po, ^{232}Th–^{228}Ra–^{228}Th and ^{235}U–^{231}Pa–^{227}Ac. These different nuclides have starkly contrasting chemistries resulting in significant elemental fractionations during a variety of magmatic processes, and their different half-lives allow the investigation of time scales ranging from less than 1 year to 10^5 years. This work builds on the dataset presented by Reagan *et al.* (1992), which investigated a limited range of U-series nuclides and was based on samples from only two eruptions. We note that the present study presents the first measurements of ^{231}Pa–^{227}Ac in volcanic samples and hence is the first time all the relevant nuclides from the ^{238}U, ^{235}U, and ^{232}Th decay series have been measured in the same lavas of a volcanic system.

BACKGROUND ON EREBUS VOLCANO

Erebus (Fig. 1) is an active composite volcano and the largest of four volcanic centers forming Ross Island: Mt. Erebus (3794 m elevation, 2170 km^3), Mt. Terror (3262 m, 1700 km^3), Mt. Bird (1800 m, 470 km^3), and Hut Point Peninsula (100 km^3). About 4520 km^3 of volcanic material has been erupted on Ross Island over the last ~4 Myr (Esser *et al.*, 2004). Ross Island is emplaced on thin (17–25 km) rifted continental crust at the southern boundary of the Terror Rift, which is a major graben located within the Victoria Land Basin on the western margin of the West Antarctic rift system (Cooper *et al.*, 1987;

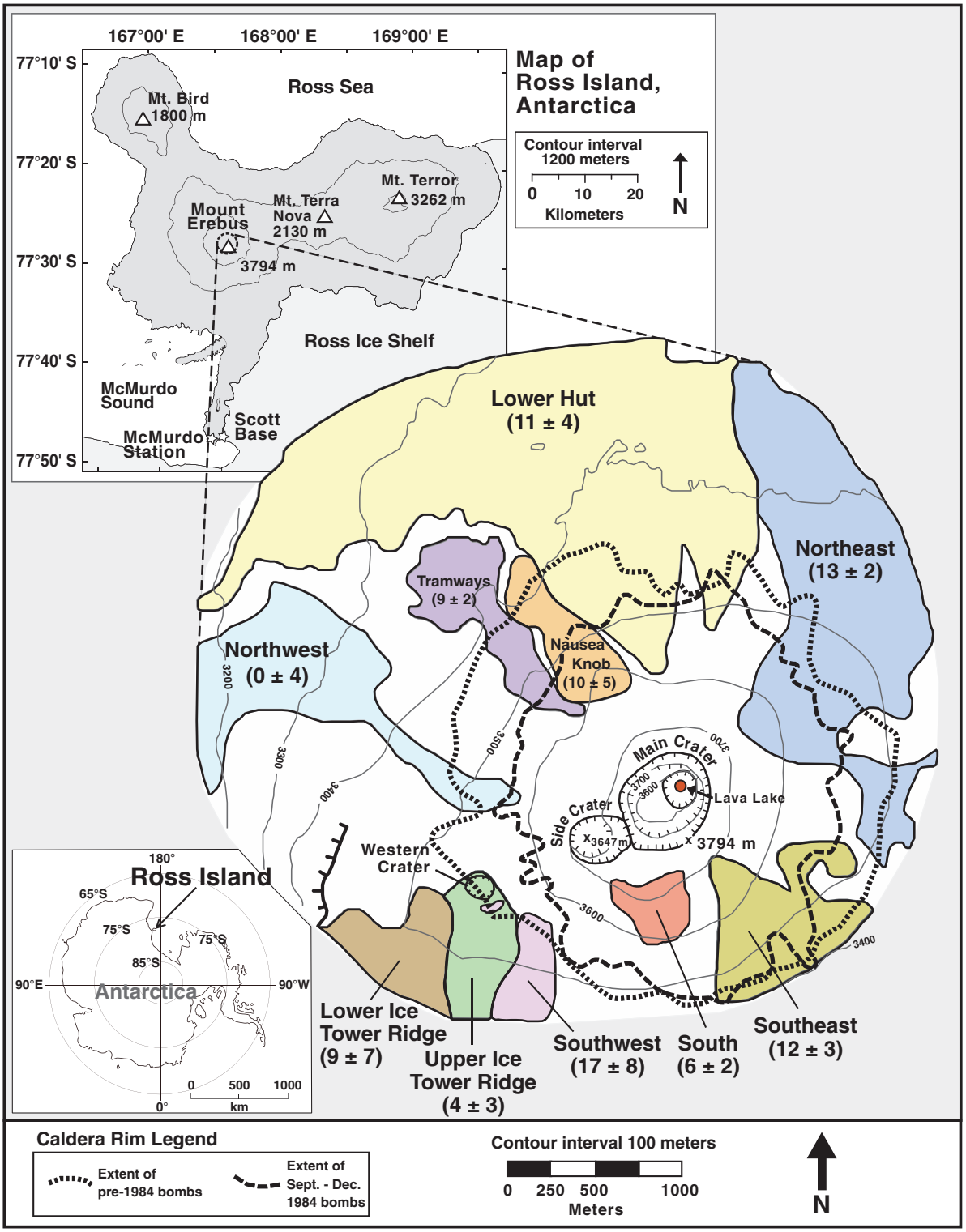

Fig. 1. Map of Mt. Erebus showing its location and the location and $^{40}Ar/^{39}Ar$ ages of its lavas. Map modified from Kelly *et al.* (2008*a*). Data taken from Harpel *et al.* (2004), Esser *et al.* (2004) and Kelly *et al.* (2008*b*).

Behrendt *et al.*, 1991; Behrendt, 1999; Bannister *et al.*, 2000; Finotello *et al.*, 2011). Late Cenozoic, intraplate, silica-undersaturated, alkaline volcanic rocks erupted on the western margin of the Ross Embayment belong to the McMurdo Volcanic Group (MVG) (Kyle, 1990*a*). In the southern Ross Sea and McMurdo Sound the MVG is referred to as the Erebus volcanic province (Kyle, 1990*b*).

The eruptive history of Erebus volcano has been divided into three distinct phases using high-precision $^{40}Ar/^{39}Ar$ dates (Esser *et al.*, 2004; Harpel *et al.*, 2004, 2008; Kelly *et al.*, 2008a): (1) a proto-Erebus shield building phase (1·3–1·0 Ma), during which basanites were erupted; (2) a proto-Erebus cone building phase (1·0 Ma–250 ka), dominated by more evolved phonotephrite lavas forming the steep slopes of the volcano; (3) the modern-Erebus cone building phase (250 ka–present), when activity increased and large volumes of anorthoclase-phyric tephriphonolite and phonolite lavas were extruded. Minor trachyte was erupted at about 170 ka during the third phase of activity (Kelly *et al.*, 2008a).

Erebus volcano has hosted a persistent convecting and degassing lava lake of anorthoclase-phyric phonolite magma for nearly 50 years. The discovery and first observations of Mt. Erebus were made in 1841 when James Ross reported it to be in a state of vigorous eruption. Subsequent, but infrequent observations made between 1841 and 1956 indicated that Erebus was actively degassing and presumably had a lava lake as the gas plume was seen to glow during the winter months. A lava lake was present in 1963 based on aerial photographs, and was first observed directly by a scientific party in December 1972 (Giggenbach *et al.*, 1973; Kyle *et al.*, 1982).

All historical eruptive volcanic activity has originated from the phonolite lava lake and adjacent vents. Variations in the style and magnitude of volcanic activity include a period of larger and more frequent Strombolian eruptions in 1984 (Kyle, 1986; Caldwell & Kyle, 1994), a phreatic eruption in 1993, and a period of almost no eruptions from 2002 to 2004. Frequent bomb ejecting Strombolian eruptions occurred through 2006 and 2007, but eruptive activity has since been quiet up to the end of 2011.

Lavas on Ross Island show two major magmatic lineages, the DVDP lineage (Kyle, 1981), named after samples from the Dry Valley Drilling Project, and the Erebus Lineage (EL) (Kyle *et al.*, 1992). The DVDP lineage lavas are older and occur at the volcanic centers surrounding Erebus volcano (Mt. Terror, Mt. Bird, and Hut Point Peninsula). They consist predominantly of basanite with minor microporphyritic kaersutite-bearing intermediate differentiates and small-volume phonolite domes. The Erebus lineage constitutes a surprisingly simple (Kyle *et al.*, 1992) and coherent fractionation trend, defined by a single liquid line of descent from basanite to phonolite with a complete sequence of intermediate (phonotephrite, tephriphonolite) eruptive products. Minor volumes of more iron-rich and less silica-undersaturated benmoreite and trachyte, termed the enriched Fe series (EFS), occur as isolated outcrops on the flanks of Erebus and adjacent islands in Erebus Bay. The EFS lavas follow a different liquid line of descent and the trachytes are interpreted to have undergone both assimilation and fractional crystallization during their evolution.

Erebus lava samples have radiogenic $^{206}Pb/^{204}Pb$ (Sun & Hansen, 1975; Sims & Hart, 2006; Sims *et al.*, 2008*a*), unradiogenic $^{87}Sr/^{86}Sr$ (Kyle *et al.*, 1992; Sims & Hart, 2006; Sims *et al.*, 2008*a*), and intermediate $^{143}Nd/^{144}Nd$ and $^{176}Hf/^{177}Hf$ (Sims & Hart, 2006; Sims *et al.*, 2008*a*), and lie along a mixing trajectory between the two end-member mantle components DMM and HIMU (Sims *et al.*, 2008*a*). The Erebus data show a marked distinction between the early-stage basanites and phonotephrites, whose Nd, Hf, Sr, and Pb isotope compositions are variable (particularly Pb), and the later, evolved phonolitic lavas and bombs, whose Nd, Hf, Sr, and Pb isotope compositions are essentially invariant (Sims *et al.*, 2008*a*). Taken together, the Erebus lineage lavas define a trend of decreasing isotopic variability with increasing extent of differentiation, indicating that magma homogenization has played a fundamental role in establishing the isotopic and compositional uniformity of the more recent phonolites (Sims *et al.*, 2008*a*).

A unique feature of the Erebus phonolite magma is the presence of abundant large anorthoclase feldspar megacrysts. These anorthoclase feldspar crystals are striking because of their large size, complex internal zoning and abundance of melt inclusions as well as inclusions of other crystalline phases such as pyroxene, apatite, magnetite, and pyrrhotite (Dunbar *et al.*, 1994; Kelly *et al.*, 2008b). The crystals can be up to 10 cm in length (Kyle, 1977), and can contain as much as 30 vol. % of melt inclusions trapped during crystal growth (Fig. 2). The melt inclusions are over 1 mm in length, and such large inclusions are typically irregular (Dunbar *et al.*, 1994), but the crystals also contain a population of negative crystal shape inclusions that are 10–40 μm in diameter. Populations of melt inclusions are trapped along what appear to be growth zones in the crystals, producing a banded appearance in backscattered electron (BSE) images. The anorthoclase crystals are complexly compositionally zoned at a number of scales and also show evidence of periods of resorption during crystal growth (Dunbar *et al.*, 1994; Kelly *et al.*, 2008b; Sumner, 2007). The compositional range of anorthoclase is $An_{10–23}$ $Ab_{62–68}$ $Or_{11–27}$ (Kelly *et al.*, 2008b). The coarsest scale of compositional zoning is defined by high- and low-Ca zones in the crystal, as illustrated by the low-Ca core and high-Ca rim of the crystal shown in Fig. 2. This zoning is attributed to either convective processes (Kelly *et al.*, 2008b) or boundary layer effects during

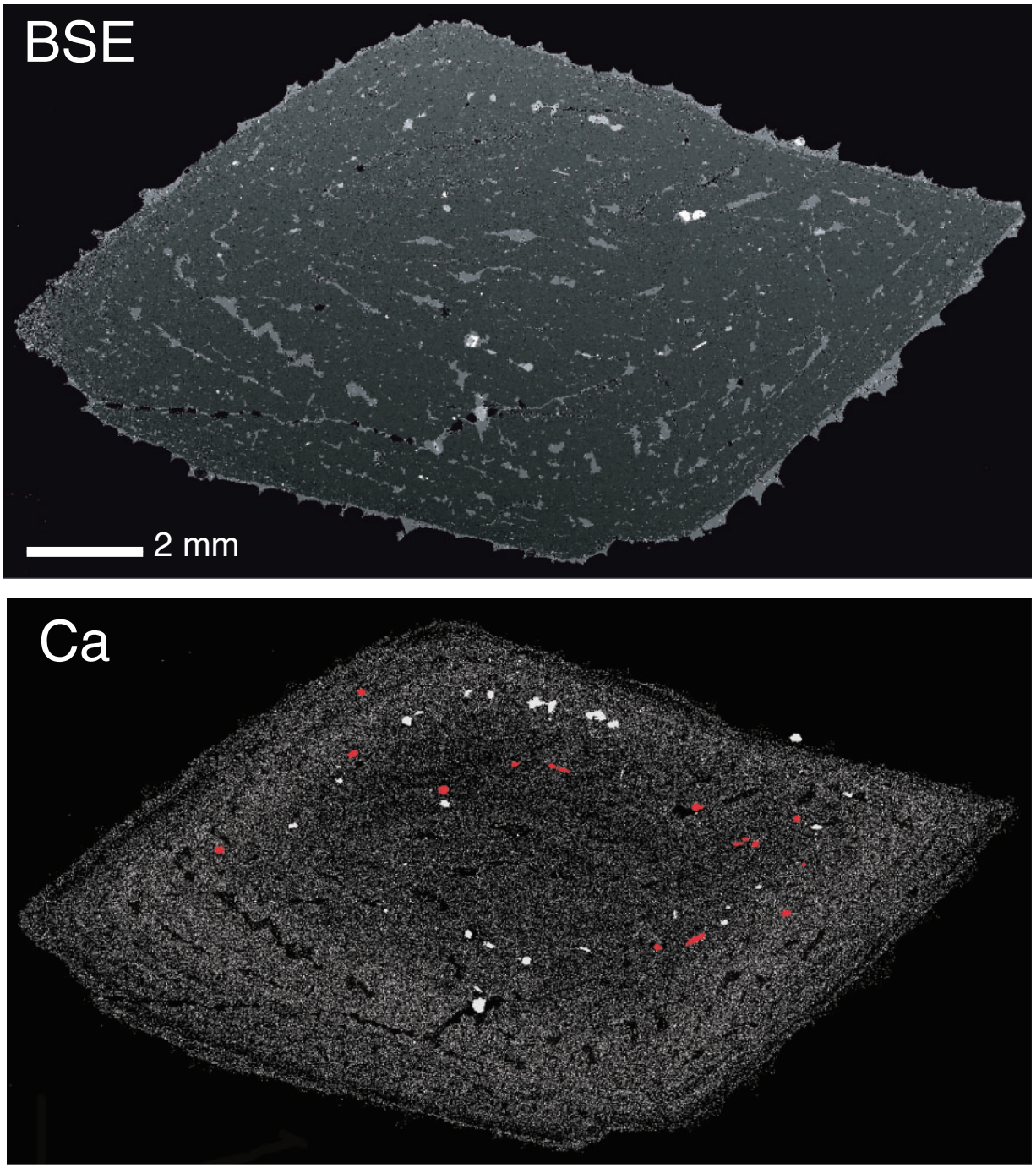

Fig. 2. Backscattered electron image (BSE) and Ca element map of a single anorthoclase crystal. The darkest areas in the BSE image are the anorthoclase host crystal. The abundant irregular areas, slightly brighter than the anorthoclase, are melt inclusions. Other included phases are pyroxene (light grey phase on Ca map), apatite (next brightest in BSE, highlighted in red on Ca map) and magnetite (brightest in BSE, dark on Ca map). The size of the apatite crystals has been slightly increased to improve visibility.

crystallization (Sumner, 2007). The observed skeletal crystal growth can be related to rapid cooling, large degrees of undercooling, or lack of available nucleation sites (Lofgren, 1980). The same effects that cause skeletal growth also tend to cause rapid crystal growth, suggesting that the Erebus anorthoclase crystals grew rapidly. Crystal size distributions, internal crystal structures and geochemical compositions (Dunbar *et al.*, 1994) suggest that the crystals have low nucleation rates but underwent rapid growth in two or more stages. The initial growth

stage produced spongy inclusion-rich cores, which were then overgrown by finely laminated rims. The composition of melt inclusions in the anorthoclase is very similar to that of the glass that forms the matrix of the samples, suggesting that the anorthoclase crystals formed in a fully evolved phonolitic melt. Assuming that the growth rate of crystals was similar to that of normal plagioclase, the age of an average Erebus anorthoclase crystal would be 100–300 years (Dunbar *et al.*, 1994). This age span would be less if the crystals grew faster, but the presence of dissolution within the crystals suggests that a simple size distribution–age calculation may underestimate the true crystal age.

Melt inclusions found in the anorthoclase crystals contain lower concentrations of H_2O, CO_2 and S (Oppenheimer *et al.*, 2011) than the assumed parental basanites. Oppenheimer *et al.* (2011) suggested that CO_2 contents in the anorthoclase melt inclusions are consistent with entrapment at pressures of up to 3 kbar. This contrasts with earlier interpretations (Dunbar *et al.*, 1994) based on H_2O contents of melt inclusions that implied that crystals growth took place either in a degassed magma in the upper (<400 m) part of the magmatic system or in degassed magma that had circulated to depth by convection in the magma conduit. Seaman *et al.* (2006) reported variable H_2O abundances in anorthoclase melt inclusions and showed ~50 μm thick zones of elevated H_2O contents on the boundary of crystals, and suggested that water diffused into crystals from melt inclusions.

In addition to containing large anorthoclase feldspar crystals, the Erebus magma also contains titanomagnetite, clinopyroxene, apatite, pyrrhotite and olivine (Kyle, 1977; Kelly *et al.*, 2008b). The textural relationships between these phases suggest that the pyroxene, titanomagnetite and olivine crystallized first. The H_2O contents of melt inclusions in pyroxene ($n=4$, $H_2O=0{\cdot}1\pm0{\cdot}05$ wt %) led Dunbar *et al.* (1994) to suggest that they crystallized high in the magmatic system.

There have been two prior studies measuring U-series disequilibria in Erebus lavas. Reagan *et al.* (1992) used ^{238}U–^{230}Th–^{226}Ra disequilibria to constrain the magma residence times for anorthoclase–glass separates from bombs erupted in 1984 and 1988. Those workers showed that the anorthoclase crystals were strongly enriched in ^{226}Ra over ^{230}Th, whereas glass separates had ^{226}Ra deficits. Based on the assumption that during crystal growth $D_{Ra}=D_{Ba}$ for anorthoclase and glass, they constructed $(^{226}Ra)/Ba$ vs $(^{230}Th)/Ba$ isochrons for the two samples and obtained two-point isochron ages of 2520 years for the 1984 sample and 2225 years for the 1988 sample. Using the activity of ^{228}Th as a proxy for ^{228}Ra (which is reasonable given the short half-life of ^{228}Th), Reagan *et al.* (1992) also measured significant $(^{228}Th/^{232}Th)$ disequilibrium in the anorthoclase [~2·16, whereas the glasses were in equilibrium with $(^{228}Th)/(^{232}Th)$ of 1·0]. Because of the short half-life of ^{228}Ra ($t_{1/2}=5{\cdot}77$ years) this result would seem to suggest that the anorthoclase crystals grew recently and rapidly. To reconcile this conundrum, Reagan *et al.* (1992) proposed that the ^{228}Th disequilibria resulted from the presence of young rims with ^{228}Ra excesses, whereas the majority of the crystals were older and had ^{228}Th–^{228}Ra–^{232}Th equilibria.

The second U-series study was by Sims & Hart (2006), who measured ^{238}U–^{230}Th disequilibria in four historical Erebus bombs as part of a global study evaluating U-series disequilibria and Nd, Sr, and Pb isotope systematics in oceanic basalts. Their results showed that the $(^{230}Th/^{232}Th)$ and $(^{238}U/^{232}Th)$ values of Erebus bombs are intermediate relative to those of other ocean island and mid-ocean ridge basalts, and form the end-member HIMU mantle component on plots of Pb isotopes versus $(^{230}Th/^{232}Th)$ and $(^{238}U/^{232}Th)$. Although Erebus does not constitute the HIMU end-member mantle component, there are no samples young enough for ^{238}U–^{230}Th disequilibria studies from Mangaia–Tubuai (the HIMU end-member); hence, for the ^{238}U–^{230}Th isotope system, Erebus, by necessity, represents the best end-member approximation of the HIMU source. Finally, it is important to note that in both studies $(^{230}Th/^{238}U)$ is >1, indicating that garnet was a residual phase during the mantle partial melting that led to the parental basanites, which in turn fractionated to form the phonolite.

SAMPLE COLLECTION AND PREPARATION

This study examines phonolite lava bombs erupted during Strombolian eruptions over a 34 year period, from 1972 to 2005. The bombs were collected on the summit crater rim or from the floor of the Main Crater.

The exact date and time of eruptions are known for some bomb samples (Table 1), whereas the young ages for other samples were determined based on their 'fresh appearance' at the time of collection. Recently erupted bombs have a distinctive metallic to iridescent vitreous luster that is quickly lost (~1–2 weeks) upon exposure to the acidic gases emitted from the lava lake and surrounding fumaroles. Therefore, for samples without eruption dates, their fresh appearance suggested they had been erupted within less than 1 or 2 months prior to collection.

Our sample suite consists of 22 bombs and five anorthoclase megacrysts separated from bombs erupted in 1984, 1989, 1993, 2004 and 2005. All samples are purified glass or anorthoclase separates. Lava bombs were disaggregated and phenocrysts and glasses were separated by handpicking to obtain ~20–30 g of each phase and subsequently purified using magnetic separation. The anorthoclase megacrysts were abraded by hand grinding to remove exterior glass. The handpicked separates (both anorthoclase

Table 1: $^{230}Th/^{232}Th$, $^{234}U/^{238}U$ and U, Th, ^{226}Ra, ^{231}Pa and Ba concentrations measured by mass spectrometry

Sample	Eruption date	[Th]† (μg g^{-1})	2σ§	[U]† (μg g^{-1})	2σ§	($^{238}U/^{232}Th$)‡	2σ§	($^{230}Th/^{232}Th$)*‡	2σ§
Glass									
ER 25724G (A1)	12/26/72	30·87	0·18	8·95	0·03	0·879	0·008	0·984	0·006
ER 2E2G (A1)	Dec-74	31·03	0·20	8·97	0·04	0·877	0·009	0·987	0·006
ER 77016G (A1)	Nov-77	31·82	0·19	9·23	0·04	0·880	0·009	0·985	0·006
ER 79302G (A1)	12/26/79	30·91	0·17	8·96	0·04	0·879	0·009	0·985	0·006
ER 82416G (A1)	Dec-82	31·73	0·17	9·16	0·03	0·875	0·008	0·986	0·006
ER 83220G (A1)	Dec-83	30·64	0·18	9·01	0·03	0·892	0·008	0·985	0·006
ER 83220G (B1)								0·987	0·009
ER 83220G (C1)								0·987	0·005
ER 84501G (A1)	Dec-84	29·14	0·19	8·50	0·04	0·885	0·009	0·979	0·006
ER 84501G (C1)									
ER 84505G (A1)	Dec-84	29·35	0·15	8·49	0·04	0·877	0·008	0·976	0·006
ER 84505G (B1)								0·973	0·009
ER 84505G (B2)								0·979	0·009
ER 84505G (B3)								0·975	0·010
ER 84505G (B4)								0·979	0·009
ER 84505G (B5)								0·976	0·010
ER 85010G (A1)	Dec-85	29·46	0·18	8·54	0·04	0·879	0·009	0·987	0·007
ER 85010G (B1)								0·983	0·010
ER 85010G (C1)								0·985	0·006
ER 86022-1G (A1)	12/22/86	30·46	0·17	8·84	0·04	0·880	0·009	0·986	0·007
ER 86022-1G (B1)								0·986	0·010
ER 88104-G (A1)	Dec-88	29·37	0·17	8·56	0·03	0·884	0·008	0·987	0·006
ER 89001G (A1)	Dec-89	29·28	0·17	8·49	0·04	0·880	0·009	0·989	0·006
ER 89001G (B1)								0·989	0·009
ER 89001G (D1)		26·28	0·14	7·77	0·03	0·897	0·008	0·976	0·003
ER 89001G (D2)		26·39	0·14	7·78	0·03	0·894	0·008	0·976	0·004
ER 89001G (D3)		27·23	0·14	8·09	0·03	0·901	0·008	0·984	0·003
ER 89001G (D4)		26·47	0·14	7·81	0·06	0·895	0·011	0·977	0·003
ER 91101G (A1)	Jan-91	29·04	0·19	8·46	0·04	0·884	0·010	0·985	0·006
ER 91101G (A2)		30·70	0·16	8·81	0·03	0·871	0·008	0·989	0·006
Er 92KSG (A1)	12/10/92	31·16	0·16	9·00	0·04	0·876	0·008	0·988	0·006
Er 92KSG (C1)								0·987	0·006
ER 93 JCG (A1)	Jan-93	29·53	0·17	8·51	0·04	0·874	0·009	0·987	0·006
ER 96 G (A1)	Dec-96	30·46	0·17	8·83	0·04	0·880	0·009	0·988	0·006
Er 97G (A1)	Dec-97	30·78	0·16	8·817	0·03	0·869	0·007	0·985	0·006
Er 99G (A1)	Dec-99	26·58	0·18	7·657	0·04	0·874	0·010	0·980	0·006
Er 99G (A2)		26·96	0·18	7·698	0·03	0·866	0·009	0·983	0·006
Er 2000 'Y2K'G (A1)	Dec-00	29·01	0·18	8·298	0·03	0·868	0·008	0·984	0·006
ER 2001G (A1)	Dec-01	29·52	0·15	8·526	0·03	0·876	0·008	0·983	0·006
ER Jan2004G (A1)	Jan-04	30·46	0·17	8·768	0·04	0·873	0·008	0·983	0·006
ER Jan2004G (C1)								0·983	0·005
ER Dec2005G (A1)	12/16/05	29·07	0·19	8·40	0·04	0·877	0·010	0·981	0·006
ER Dec2005G (C1)								0·980	0·005
ER Dec2005G (D1)		22·20	0·12	6·419	0·021	0·877	0·008	0·970	0·006
Anorthoclase megacrysts									
84 xyll (A1)	1984	0·28	0·003	0·07	0·001	0·765	0·015	0·977	0·006
88 xyll (A1)	1988	0·22	0·002	0·06	0·001	0·771	0·015	0·980	0·006
93 xyll (A1)	1993	0·19	0·002	0·05	0·000	0·778	0·016	0·981	0·006
04 xyll (A1)	2004	0·23	0·002	0·06	0·001	0·782	0·016	0·981	0·006
05 xyll (A1)	2005	0·27	0·003	0·07	0·001	0·780	0·016	0·982	0·006

(continued)

Table 1: Continued

Sample	Eruption date	[Th]† (μg g^{-1})	2σ§	[U]† (μg g^{-1})	2σ§	(^{238}U/^{232}Th)‡	2σ§	(^{230}Th/^{232}Th)*‡	2σ§
Quality assurance standards‖									
TML (A) (n = 22; #dis. = 7)		30·50	0·71	10·79	0·20	1·073	0·045	1·071	0·006
ATHO (A) (n = 11; #dis. = 3)		7·44	0·03	2·26	0·05	0·920	0·022	1·017	0·005
BCR-2 (A) (n = 6; #dis. = 3)		5·89	0·03	1·71	0·02	0·879	0·015	0·874	0·005
KL-31-KWWS-92 (A) (n = 1)				0·292	0·004				
HK-04-KWWS-92 (A) (n = 1)				0·665	0·010				
Kilauea_Skylight (D) (n = 1)				0·260	0·003				

Sample	Eruption date	[^{226}Ra]† (fg g^{-1})	2σ§	(^{226}Ra/^{230}Th)‡	2σ§	[^{231}Pa]† (fg g^{-1})	2σ§	(^{231}Pa/^{235}U)‡	2σ§
Glass									
ER 25724G (A1)	12/26/72	2469	37	0·73	0·01				
ER 2E2G (A1)	Dec-74								
ER 77016G (A1)	Nov-77	2560	38	0·73	0·01				
ER 79302G (A1)	12/26/79	2480	37	0·73	0·01				
ER 82416G (A1)	Dec-82								
ER 83220G (A1)	Dec-83								
ER 83220G (B1)									
ER 83220G (C1)									
ER 84501G (A1)	Dec-84								
ER 84501G (C1)									
ER 84505G (A1)	Dec-84	2388	36	0·75	0·01				
ER 84505G (B1)									
ER 84505G (B2)									
ER 84505G (B3)									
ER 84505G (B4)									
ER 84505G (B5)									
ER 85010G (A1)	Dec-85								
ER 85010G (B1)									
ER 85010G (C1)									
ER 86022-1G (A1)	12/22/86								
ER 86022-1G (B1)									
ER 88104-G (A1)	Dec-88	2413	36	0·75	0·01				
ER 89001G (A1)	Dec-89	2306	35	0·72	0·01	3369	40	1·220	0·02
ER 89001G (B1)									
ER 89001G (D1)						2735	29	1·083	0·02
ER 89001G (D2)						3202	34	1·266	0·02
ER 89001G (D3)						3120	31	1·186	0·01
ER 89001G (D4)						2493	61	0·981	0·03
ER 91101G (A1)	Jan-91	2329	35	0·73	0·01	3481	42	1·265	0·02
ER 91101G (A2)		2369	36	0·70	0·01				
Er 92KSG (A1)	12/10/92	2300	34	0·67	0·01	3585	43	1·225	0·02
Er 92KSG (C1)									
ER 93 JCG (A1)	Jan-93	2324	35	0·72	0·01	3376	41	1·220	0·02
ER 96G (A1)	Dec-96	2332	35	0·70	0·01				
Er 97G (A1)	Dec-97	2298	34	0·68	0·01				
Er 99G (A1)	Dec-99	2283	34	0·79	0·01	3300	40	1·325	0·02
Er 99G (A2)		2300	34	0·78	0·01				
Er 2000 'Y2K'G (A1)	Dec-00	2306	35	0·73	0·01	3283	39	1·216	0·02
ER 2001G (A1)	Dec-01								
ER Jan2004G (A1)	Jan-04	2306	35	0·69	0·01	3449	41	1·209	0·02
ER Jan2004G (C1)									

(continued)

Table 1: Continued

Sample	Eruption date	[^{226}Ra]† (fg g^{-1})	2σ§	(^{226}Ra/^{230}Th)‡	2σ§	[^{231}Pa]† (fg g^{-1})	2σ§	(^{231}Pa/^{235}U)‡	2σ§
ER Dec2005G (A1)	12/16/05	2296	34	0·724	0·01				
ER Dec2005G (C1)									
ER Dec2005G (D1)						2623	28	1·256	0·02
Anorthoclase megacrysts									
84 xyll (A1)	1984	917	14	30·66	0·46				
88 xyll (A1)	1988	950	14	39·93	0·60				
93 xyll (A1)	1993	939	14	44·70	0·67				
04 xyll (A1)	2004	1000	15	39·77	0·60				
05 xyll (A1)	2005	1105	17	37·25	0·56				
Quality assurance standards[‖]									
TML (A) ($n=22$; #Dis. $=7$)		3675	110	1·01	0·05				
ATHO (A) ($n=11$; #Dis. $=3$)		847	56	1·01	0·03				
BCR-2 (A) ($n=6$; #Dis. $=3$)		565	47	0·99	0·02				
KL-31-KWWS-92 (A) ($n=1$)						103·00	1·55	1·08	0·03
HK-04-KWWS-92 (A) ($n=1$)						389·20	4·67	1·79	0·05
Kilauea_Skylight (D) ($n=1$)						92·28	0·59	1·09	0·02

Sample	Eruption date	(^{234}U/^{238}U)*‡	2σ§	Ba$^{\#}$ (μg g^{-1})	Ba-ID† (μg g^{-1})	2σ§
Glass						
ER 25724G (A1)	12/26/72	0·996	0·004	435		
ER 2E2G (A1)	Dec-74	1·002	0·004			
ER 77016G (A1)	Nov-77	1·001	0·003	461		
ER 79302G (A1)	12/26/79	1·003	0·004	454		
ER 82416G (A1)	Dec-82	0·998	0·004	445		
ER 83220G (A1)	Dec-83	1·001	0·004	463		
ER 83220G (B1)						
ER 83220G (C1)		1·001	0·003			
ER 84501G (A1)	Dec-84	1·000	0·003	455		
ER 84501G (C1)		0·997	0·003			
ER 84505G (A1)	Dec-84	1·001	0·002	465	473·5	7·1
ER 84505G (B1)						
ER 84505G (B2)						
ER 84505G (B3)						
ER 84505G (B4)						
ER 84505G (B5)						
ER 85010G (A1)	Dec-85	1·002	0·003	404		
ER 85010G (B1)						
ER 85010G (C1)		1·001	0·002			
ER 86022-1G (A1)	12/22/86	1·001	0·003	438		
ER 86022-1G (B1)						
ER 88104-G (A1)	Dec-88	1·003	0·003		512·4	7·7
ER 89001G (A1)	Dec-89	1·002	0·003	463		
ER 89001G (B1)						
ER 89001G (D1)		1·002	0·002			
ER 89001G (D2)		1·005	0·002			
ER 89001G (D3)		1·002	0·002			
ER 89001G (D4)		1·001	0·002			
ER 91101G (A1)	Jan-91	0·999	0·003	449		
ER 91101G (A2)						
Er 92KSG (A1)	12/10/92	1·002	0·002	463		
Er 92KSG (C1)		1·003	0·003			

(continued)

Table 1: Continued

Sample	Eruption date	$(^{234}U/^{238}U)^{*\ddagger}$	$2\sigma^{\S}$	$Ba^{\#}$ (μg g^{-1})	Ba-ID† (μg g^{-1})	$2\sigma^{\S}$
ER 93 JCG (A1)	Jan-93	1·002	0·002	454	502·38	7·5
ER 96G (A1)	Dec-96	1·000	0·002	436		
Er 97G (A1)	Dec-97			442		
Er 99G (A1)	Dec-99	1·001	0·002	429		
Er 99G (A2)						
Er 2000 'Y2K'G (A1)	Dec-00	0·999	0·002	405		
ER 2001G (A1)	Dec-01			475		
ER Jan2004G (A1)	Jan-04	1·002	0·002	404	486·58	7·3
ER Jan2004G (C1)		1·001	0·002			
ER Dec2005G (A1)	12/16/05	1·002	0·002		495·640	7·4
ER Dec2005G (C1)		1·001	0·002			
ER Dec2005G (D1)		1·002	0·002			
Anorthoclase megacrysts						
84 xyll (A1)	1984	1·001	0·003		2428·6	36
88 xyll (A1)	1988	1·002	0·003		2327·1	35
93 xyll (A1)	1993	0·998	0·003		2568·3	39
04 xyll (A1)	2004	1·003	0·003		2295·7	34
05 xyll (A1)	2005	1·001	0·003		2389·3	36
Quality assurance standards$^{||}$						
TML (A) ($n=22$; #dis. $=7$)		1·0007	0·003			
ATHO (A) ($n=11$; #dis. $=3$)		0·9997	0·003			
BCR-2 (A) ($n=6$; #dis. $=3$)		1·0031	0·004			
KL-31-KWWS-92 (A) ($n=1$)						
HK-04-KWWS-92 (A) ($n=1$)						
Kilauea_Skylight (D) ($n=1$)						

*U and Th isotopic compositions measured by: (A) MC-ICP-MS at WHOI using the ThermoFisher NEPTUNE (Ball *et al.*, 2008; Sims *et al.*, 2008*b*, 2008*c*); (B) SIMS at WHOI using the Cameca IMS 1270 (Layne & Sims, 2000); (C) MC-ICP-MS at Wyoming High Precision Isotope Laboratory using the ThermoFisher NEPTUNE Plus; (D) MC-ICP-MS at Bristol Isotope Group using the ThermoFisher NEPTUNE (Hoffman *et al.*, 2007).

†For concentration measurements: (A) [U], [Th], [^{226}Ra], [Ba] and [^{231}Pa] measured by ID-ICP-MS at WHOI using the ThermoFisher ELEMENT2 (Choi *et al.*, 2001; Pichat *et al.*, 2004; Sims *et al.*, 2008*b*, 2008*c*); (D) [U], [Th] and [^{231}Pa], [Ba] measured by ID-ICP-MS at Bristol using the ThermoFisher NEPTUNE (Hoffman *et al.*, 2007; Prytulak *et al.*, 2007, 2008).

‡() denotes activity. Activity ratios were calculated using $\lambda_{230}=9{\cdot}1577\times10^{-6}$ yr^{-1}, $\lambda_{234}=2{\cdot}8262\times10^{-6}$ yr^{-1}, $\lambda_{238}=1{\cdot}551\times10^{-10}$ yr^{-1}; $\lambda_{232}=4{\cdot}948\times10^{-11}$ yr^{-1}; $\lambda_{226}=4{\cdot}331\times10^{-4}$ yr^{-1}; $\lambda_{231}=2{\cdot}1158\times10^{-5}$ yr^{-1}; $\lambda_{235}=9{\cdot}8485\times10^{-10}$ yr^{-1} (Le Roux & Glendenin, 1963; Robert *et al.*, 1969; Jaffey *et al.*, 1971; Holden, 1990; Cheng *et al.*, 2000; Tuli, 2000).

§Errors (2σ) are calculated using standard error propagation methods and include uncertainties in: (1) the decay constants, λ_{230} (0·3%), λ_{232} (0·5%), λ_{238} (o·2%), λ_{238} (0·07%), λ_{232} (0·5%), λ_{226} (0·4%), λ_{231} (0·4%) or λ_{235} (0·07%) (Le Roux & Glendenin, 1963; Robert *et al.*, 1969; Jaffey *et al.*, 1971; Holden, 1990; Cheng *et al.*, 2000; Tuli, 2000); (2) the time-averaged uncertainty in ^{233}U (0·7%) ^{229}Th (1%), ^{228}Ra (1·3%) spikes used for isotope dilution; (3) the instrument parameters, including the uncertainty in determining the tailing of ^{232}Th on ^{230}Th (~0·1–0·2%); (4) the weighing errors (<0·001%); (5) measurement precision for the samples and bracketing standards (0·03–0·4%).
Inter-laboratory (i.e. WHOI, Bristol, University of Wyoming) and inter-technique (MC-ICP-MS vs SIMS) replicates come from separate powder dissolutions. Intra-laboratory and intra-technique replicates come from different chemical processing of a single dissolution.

||TML, ATHO and BCR2 were measured for quality assurance. Values reported here represent the range of values measured for (^{238}U/^{232}Th), (^{230}Th/^{232}Th) (^{230}Th/^{238}U), [^{226}Ra] and (^{226}Ra/^{230}Th) over the period of this study from ~1999 to now. The table lists both the number of analyses and dissolutions incorporated into these numbers. Replicates for synthetic rock and standards run over the same time interval and their comparison with results from other laboratories has been reported by Layne & Sims (2000), Ball *et al.* (2007) and Sims *et al.* (2008*b*, 2008*c*). For the WHOI (^{231}Pa/^{235}U) measurements two Hawaiian samples, KL-31-KWWS-92 and HK-04-KWWS-92, were measured for quality assurance during the same time as these analyses; these measurements agree, within error, with the reported values for these same samples given by Sims *et al.* (1999) [see also Sims *et al.* (2008*c*)]. For Bristol's (^{231}Pa/^{235}U) measurements, Hawaiian sample Kilauea Skylight (collected from a skylight of a Pu'u O'o flow by Dave Sherrod on 16 May 1996 was measured and gives a (^{231}Pa/^{235}U) very similar to other historical Kilauea Pu'u O'o samples measured by Sims *et al.* (1999) and KL-31-KWWS-92 measured here.

#Ba concentrations from standard ICP-MS come from Kelly *et al.* (2008b).

and phonolite glass) were then ground to <0·04 mm and magnetically separated using a Frantz magnetic separator. Magnetic separation was repeated until visually clean separates of anorthoclase (melt inclusion free) and purified glass were obtained.

All glass samples have previously been characterized for their major and trace element abundances (Kelly *et al.*, 2008*b*) and long-lived radiogenic Nd, Sr, Hf and Pb isotope compositions (Sims & Hart, 2006; Sims *et al.*, 2008*a*).

ANALYTICAL METHODS

^{238}U, ^{232}Th and ^{235}U decay series

The anorthoclase separates and glasses were dissolved in a series of digestions using concentrated HF and HNO_3, followed by $HNO_3 + H_3BO_3$ and $HClO_4$ to break down all fluorides. Care was taken to ensure complete digestion and elimination of all fluorides.

^{238}U, ^{232}Th, ^{235}U, ^{227}Ac, ^{226}Ra, ^{210}Pb, ^{210}Po, and ^{228}Ra concentrations and $^{234}U/^{238}U$ and $^{230}Th/^{232}Th$ isotopic ratios were measured by a combination of multi-collector inductively coupled plasma mass spectrometry (MC-ICP-MS) ($^{234}U/^{238}U$ and $^{230}Th/^{232}Th$), secondary ionization mass spectrometry (SIMS) ($^{230}Th/^{232}Th$), isotope dilution (ID) mass spectrometry (^{232}Th, ^{238}U, ^{231}Pa, ^{226}Ra and Ba concentrations), gamma spectrometry (^{214}Pb and ^{214}Bi as proxies for ^{226}Ra, and ^{228}Ac and ^{208}Tl as proxies for ^{228}Ra), and alpha spectrometry (^{210}Po as a proxy for ^{210}Pb for older samples and as a direct measure of ^{210}Po, and ^{228}Th as a proxy for ^{228}Ra and ^{227}Ac). Details of the methods for these measurements have been given in published analytical and interpretative papers (Choi *et al.*, 2001; Layne & Sims, 2000; Pichat *et al.*, 2004; Reagan *et al.*, 2006, 2008; Ball *et al.*, 2008; Hoffman *et al.*, 2007; Prytulak *et al.*, 2008; Prytulak & Elliott, 2009; Sims *et al.* 2008*b*, 2008*c*). Details of the ^{227}Ac method are given in Appendix A and were published by Dulaiova *et al.* (2012). The ^{228}Th method is also described in Appendix A. Tables 1–3 tabulate the data and provide information on relevant details such as the decay constants used and the method of error propagation.

In situ analysis of anorthoclase megacrysts, apatite and trapped melt inclusions

We measured Ba and Th concentrations in two 1984 and one 1988 Erebus anorthoclase megacrysts and their melt inclusions by SIMS (IMS-3f, Cameca) at the Northeast National Ion Microprobe Facility at the Woods Hole Oceanographic Institution (Table 4). The megacrysts were cut perpendicularly to their elongated axis. The polished sections of the samples were Au-coated. The analyses were made using a negatively charged oxygen ion (O^-) beam with a net voltage of 12·5 kV. The beam diameter was 10 μm. Molecular ion interferences were suppressed using an energy filtering technique (Shimizu & Hart, 1982*a*, 1982*b*) by offsetting the secondary accelerating voltage by 100 V. The ^{138}Ba and ^{232}Th counts were normalized to ^{30}Si. We used four reference glasses to calibrate the ion microprobe (NIST610, NIST612, KL2G and ML3G) to obtain the empirical relationships between the concentrations of Ba and Th and the element/^{30}Si ratio (e.g. Shimizu & Hart, 1982*a*, 1982*b*). The Ba and Th concentrations used for these glass standards are from the GeoREM database (Jochum *et al.*, 2005). The calculated concentrations were within 7% and 13% of the certified values, respectively. Major element compositions were measured on the same crystal sections using a Cameca SX100 electron microprobe at New Mexico Tech. For the feldspar analyses, we used an accelerating voltage of 15 kV and a probe current of 20 nA, with the beam broadened to 10 μm to avoid Na loss. Count times for all elements were 20 s on peak and 10 s on background, with the exception of Sr and Ba, for which peak count times of 60 s were used, and 30 s background count times. We used the average SiO_2 concentration measured by electron microprobe in the melt inclusions or in the anorthoclase to calculate the Th and Ba concentrations. The precision on SiO_2 determinations, based on replicate analysis of standard reference materials, averaged ±0·35 wt %.

Quantitative analyses of the Th (and U and Pb) contents of apatite inclusions in the anorthoclases were also carried out using the Cameca SX100 electron microprobe at New Mexico Tech. A standard accelerating voltage of 15 kV was used, but because of the low abundances of these elements in apatite, high probe currents (200 nA) and long peak count times (300–400 s) were used. Uranium and Pb abundances in apatite inclusions in the anorthoclases were below instrumental detection limits.

RESULTS

^{238}U, ^{232}Th, ^{235}U, ^{227}Ac, ^{226}Ra, ^{210}Pb, ^{210}Po, and ^{228}Ra concentrations and ($^{234}U/^{238}U$), ($^{230}Th/^{232}Th$), ($^{230}Th/^{238}U$), ($^{226}Ra/^{230}Th$), ($^{235}U/^{231}Pa$), ($^{231}Pa/^{227}Ac$), and ($^{228}Ra/^{232}Th$) are reported in Tables 1–3 and shown in Figs 3–8.

For quality assurance, replicate measurements of ($^{238}U/^{232}Th$), ($^{230}Th/^{232}Th$), ($^{230}Th/^{238}U$), ($^{234}U/^{238}U$), ($^{226}Ra/^{230}Th$), ($^{235}U/^{231}Pa$), and ($^{231}Pa/^{227}Ac$) were conducted for the rock standards ATHO and TML (Table 1); these analyses are consistent, within analytical uncertainties, with expectations of equilibrium, and also with previously reported MC-ICP-MS, thermal ionization mass spectrometry (TIMS) and SIMS measurements (see Sims *et al.*, 2008*a*).

^{238}U decay series

^{238}U–^{234}U–^{230}Th

U and Th concentrations and ($^{234}U/^{238}U$) and ($^{230}Th/^{232}Th$) (^{234}U $t_{1/2} = 245\,250$ years and ^{230}Th $t_{1/2} = 75\,690$ years) were measured in the 22 historical phonolite bombs and five

Table 2: Short-lived gamma counting data ^{226}Ra proxies (^{214}Pb and ^{214}Bi), ^{210}Pb, and ^{228}Ra proxies (^{228}Ac and ^{208}Tl)

Sample	Eruption date	ID-ICP-MS ^{226}Ra (d.p.m. g^{-1})	ID-ICP-MS ^{232}Th (d.p.m. g^{-1})	(^{214}Pb) (d.p.m. g^{-1})	1σ RSD (%)	($^{214}Pb/^{226}Ra$)	(^{214}Bi) (d.p.m. g^{-1})	1σ RSD (%)	($^{214}Bi/^{226}Ra$)
Glass									
84505G	1984	5·24	7·17	5·26	0·01	1·00	5·13	0·02	0·98
91101G	1991	5·15	7·09	4·99	0·01	0·97	4·92	0·02	0·96
Er 92KS-G	1992	5·05	7·61	5·05	0·02	1·00	5·13	0·03	1·02
ER 93 JC	1993	5·10	7·21	5·06	0·01	0·99	4·94	0·02	0·97
Er 96G	1996	5·12	7·44	5·06	0·01	0·99	5·12	0·02	1·00
Er 97G	1997	5·04	7·51	5·20	0·01	1·03	5·11	0·02	1·01
Er 99G	1999	5·03	6·54	5·02	0·01	1·00	5·05	0·02	1·00
Er 2000 'Y2K'G	2000	5·06	7·08	5·11	0·01	1·01	5·06	0·02	1·00
JAN2004G	2004	5·06	7·44	5·17	0·01	1·02	5·08	0·02	0·98
Dec-05	2005	5·04	7·10	5·16	0·01	1·02	5·09	0·02	0·98
Anorthoclase megacrysts									
84 xyll	1984	2·01	0·067	1·94	0·03	0·96	b.d.		
93 xyll	1993	2·06	0·047	2·12	0·03	1·03	b.d.		
04 xyll	2004	2·19	0·056	2·22	0·03	1·01	2·081	0·04	0·98
05 xyll	2005	2·42	0·066	2·60	0·02	1·07	2·470	0·02	0·98

Sample	Eruption date	(^{210}Pb) (d.p.m. g^{-1})	1σ RSD (%)	($^{210}Pb/^{226}Ra$)	(^{228}Ac) (d.p.m. g^{-1})	1σ RSD (%)	($^{228}Ac/^{232}Th$)	(^{208}Tl) (d.p.m. g^{-1})	1σ RSD (%)	($^{208}Tl/^{232}Th$)
Glass										
84505G	1984	4·84	0·06	0·92	7·20	0·02	1·00	6·98	0·02	0·97
91101G	1991	5·26	0·04	1·02	6·99	0·02	0·99	6·89	0·02	0·97
Er 92KS-G	1992	4·96	0·08	0·98	7·50	0·04	0·99	7·46	0·03	0·98
ER 93 JC	1993	4·94	0·05	0·97	7·15	0·02	0·99	7·00	0·02	0·97
Er 96G	1996	5·30	0·05	1·04	7·18	0·02	0·97	7·16	0·02	0·96
Er 97G	1997		0·04		7·30	0·02	0·97	7·19	0·02	0·96
Er 99G	1999	4·86	0·05	0·97	6·40	0·02	0·98	6·45	0·02	0·99
Er 2000 'Y2K'G	2000	4·82	0·05	0·95	6·86	0·02	0·97	6·90	0·02	0·97
JAN2004G	2004	4·91	0·05	0·97	7·14	0·02	0·96	7·12	0·02	0·96
Dec-05	2005	4·80	0·05	0·95	6·88	0·02	0·97	6·87	0·02	0·97
Anorthoclase megacrysts										
84 xyll	1984	2·05	0·12	1·02	b.d.			b.d.		
93 xyll	1993	2·27	0·11	1·10	b.d.			b.d.		
04 xyll	2004	2·35	0·12	1·07	b.d.			b.d.		
05 xyll	2005	2·65	0·09	1·10	b.d.			b.d.		

ATHO is used to calibrate efficiencies for 46·52 keV (^{210}Pb), 338·4 keV (^{228}Ac), 351·99 keV (^{214}Pb), 583·14 keV (^{208}Tl), and 609·32 keV (^{214}Bi).
Branching ratios used are 0·0405 for 46·52 keV (^{210}Pb), 0·1136 for 338·4 keV (^{228}Ac), 0·372 for 351·99 keV (^{214}Pb), 0·8423 for 583·14 keV (^{208}Tl), and 0·4628 for 609·32 keV (^{214}Bi).
Comparing samples sealed in epoxy with samples that were not checked for Rn degassing. The two approaches give equivalent concentrations.
(^{228}Ra) and (^{232}Th) activities calculated from mass spectrometry data (Table 1).
b.d., below detection limit.

Table 3: Short-lived alpha counting data for ^{210}Po, ^{227}Ac and ^{228}Th

Sample	Date of analysis	(^{226}Ra) ID-ICP-MS* (d.p.m. g^{-1})	(^{210}Po)† (d.p.m. g^{-1})	2σ	(^{210}Po/^{226}Ra)$_0$	Date of analysis	(^{230}Th/^{232}Th)	2σ	(^{228}Th/^{232}Th)°	2σ
ER 84505 (An)	8/4/06	2·01	1·99	0·08	0·989					
ER 91101 (Gl)	6/27/06	5·15	5·26	0·2	1·021					
ER 92KS (Gl)	6/27/06	5·05	5·27	0·2	1·044					
ER 93 JC (An)	8/4/06	2·06	2·09	0·08	1·014					
ER 96 (Gl)	6/27/06	5·12	5·27	0·22	1·030					
ER 99 (Gl)	6/16/06	5·03	5·26	0·21	1·046					
ER 2000 (Gl)	6/16/06	5·06	5·12	0·19	1·012					
ER Jan2004 (Gl)	2/7/07	5·06	5·06	0·16	1·000					
	3/23/07	5·06	5·34	0·2	1·055					
ER Jan2004 (An)	5/26/06	2·19	2·22	0·09	1·012					
ER Dec2005 (Gl)	5/26/06		3·65	0·14						
	2/7/07		4·82	0·16						
	4/4/08	5·04	5·3	0·16	1·052					
ER Dec2005 (An)	5/26/06	2·42	2·42	0·1	0·998	4/27/2008	0·91	0·13	1·41	0·2
Quality assurance										
BCR-2										
BCR-2 (Bristol)‡										
SAV-B6										
(1901 Samoa Flow)										

Sample	(^{231}Pa) ID-ICPMS* (d.p.m. g^{-1})	2σ	Date of analysis	(^{227}Ac) (d.p.m. g^{-1})	2σ	(^{227}Ac/^{231}Pa)	2σ
ER 84505 (An)							
ER 91101 (Gl)							
ER 92KS (Gl)							
ER 93 JC (An)							
ER 96 (Gl)							
ER 99 (Gl)	0·346	0·01	6/10/00	0·3498	0·02	1·01	0·06
ER 2000 (Gl)							
ER Jan2004 (Gl)							
ER Jan2004 (An)	0·362	0·01	9/9/07	0·36815	0·02	1·02	0·06
ER Dec2005 (Gl)							
ER Dec2005 (An)							
Quality assurance							
BCR-2	0·057	0·002		0·058	0·003	1·02	0·06
BCR-2 (Bristol)‡	0·058	0·0006		0·058	0·003	1·03	0·05
SAV-B6 (1901 Samoa Flow)	0·041	0·001		0·0406	0·002	1·00	0·06

*(^{226}Ra) and (^{231}Pa) are measured by ID-ICP-MS (Table 1).
†^{210}Po alpha counts are decay corrected to the date of ^{210}Pb–^{210}Po separation.
‡^{231}Pa activity comes from average BCR-2 concentration of 550·3 ± 7·2 (2σ standard deviation; $n = 15$) from Prytulak *et al.* (2008).

Table 4: Average in situ Ba and Th concentrations in anorthoclase megacrysts and their melt inclusions measured by SIMS (IMS-3f Cameca) at WHOI

	Ba		Th	
	(μg g^{-1})	1σ	(μg g^{-1})	1σ
ER84-01				
Melt inclusion	490	90	31·7	4·4
Anorthoclase	2185	291	0·10	0·04
ER84-04				
Melt inclusion	549	31	28·0	3·3
Anorthoclase	2279	47	0·03	0·02
ER88-01				
Melt inclusion	410	18	24·66	2·36
Anorthoclase	1840	54	0·13	0·07

These data are averages from multiple spot measurements (see Table A1).

anorthoclase megacrysts (Table 1 and Figs 3 and 4). Replicate analyses for the mass spectrometric techniques (SIMS versus MC-ICP-MS) and the different laboratories (WHOI, University of Wyoming, Bristol) are reported in Table 1. All of the samples analyzed in this study have (^{234}U/^{238}U) activity ratios of unity (±4 per mil) (Table 1). (^{230}Th/^{232}Th) and (^{238}U/^{232}Th) for all of the historical Erebus bombs are uniform within analytical uncertainties and (^{230}Th/^{238}U) is greater than one, indicating that daughter ^{230}Th has been enriched relative to its parent ^{238}U [hereafter (^{230}Th/^{238}U) >1 is referred to as ^{230}Th excess]. For the anorthoclase megacrysts, ^{230}Th/^{232}Th is identical to the glass separates from the same bombs, but (^{238}U/^{232}Th) is lower and (^{230}Th/^{238}U) is higher (Table 1; Figs 3 and 4).

For the ^{230}Th/^{232}Th measurements, inter- and intra-technique reproducibility (SIMS and MC-ICP-MS) and inter-laboratory reproducibility (University of Wyoming, Bristol and WHOI) are within analytical error, which is less than 1%. For (^{238}U/^{232}Th), inter-laboratory (Bristol versus WHOI) reproducibility is also within analytical error, again less than 1%; however, the Bristol measurements give significantly lower U and Th concentrations than the WHOI results. We interpret the lower U and Th concentrations in the Bristol Isotope Group measurements as variable amounts of admixed anorthoclase megacrysts, as the Bristol laboratory received whole-rock phonolite bomb samples. Anorthoclase has extremely low U and Th concentrations (Table 1). Simple mixing calculations between average phonolite glass and anorthoclase (Table 5) show that incorporation of 20% crystals in the phonolite glass aliquots (which is less than their modal abundances of ~30%) will lower the concentrations of U and Th by about 20%. This is comparable with the Bristol measurements and changes the (^{238}U/^{232}Th) of the samples by only 0·02%. We further note that U and Th concentrations also have been measured in purified glass separates by standard ICP-MS (Kelly *et al.*, 2008b) and are similar, within analytical uncertainties, to the WHOI isotope dilution measurements.

For the 1984 bomb, (^{238}U/^{232}Th) and (^{230}Th/^{232}Th) are similar, within analytical uncertainty, to the values reported by Reagan *et al.* (1992). However, for the 1988 bomb the (^{230}Th/^{232}Th) reported by Reagan *et al.* (1992) is higher than our values by 2% for the glass and 5% for the anorthoclase, and the (^{238}U/^{232}Th) is higher than our values by 4% for the glass and 10% for the anorthoclase. Because our data give horizontal isochrons, are remarkably uniform for the 34 year sample suite, and have been measured in multiplicity by newer mass spectrometric methods and by different laboratories, we consider these newer data to be the most reliable.

^{230}Th–^{226}Ra

^{226}Ra ($t_{1/2}$ = 1600 years) concentrations were measured in glass separates from 15 historical phonolite bombs and five anorthoclase megacryst separates (Table 1, Fig. 5). For the bombs (^{226}Ra/^{230}Th) is <1 and relatively uniform for the glass separates (0·722 ± 0·057, 2σ), whereas for the anorthoclase separates (^{226}Ra/^{230}Th) ranges from 30·6 to 40·7. These values are consistent with the (^{226}Ra/^{230}Th) measured for the glass and anorthoclase in 1984 and 1988 bombs by Reagan *et al.* (1992).

^{226}Ra was measured by both isotope dilution mass spectrometry using MC-ICP-MS and gamma counting of the short-lived ^{226}Ra daughters ^{214}Pb and ^{214}Bi (Sims *et al.*, 2008*b*). This latter approach assumes that (^{226}Ra) is in radioactive equilibrium with (^{214}Pb) and (^{214}Bi), which is reasonable given the extremely short half-lives of these daughter nuclides (35 ms to 3·83 days). Within their respective analytical uncertainties, both daughter activities give concurrent results amongst themselves and with the mass spectrometric ^{226}Ra measurements (Tables 1 and 2).

^{226}Ra–^{210}Pb

^{210}Pb ($t_{1/2}$ = 22·6 years) was measured by gamma spectroscopy and by ^{210}Po ingrowth using alpha spectrometry (Figs 6 and 7; Tables 2 and 3). Although the ^{210}Po alpha counting data are more precise and accurate, both methods give equivalent results within their respective analytical uncertainties. All samples measured in this study are in equilibrium with regard to ^{210}Pb–^{226}Ra (Fig. 6).

^{210}Pb–^{210}Po

For the 2005 sample (erupted on 16 December 2005) ^{210}Po ($t_{1/2}$ = 138·4 days) was measured by alpha spectrometry in three aliquots over a 1 year period (Table 3; Fig. 7). In most magmas, complete polonium volatilization occurs

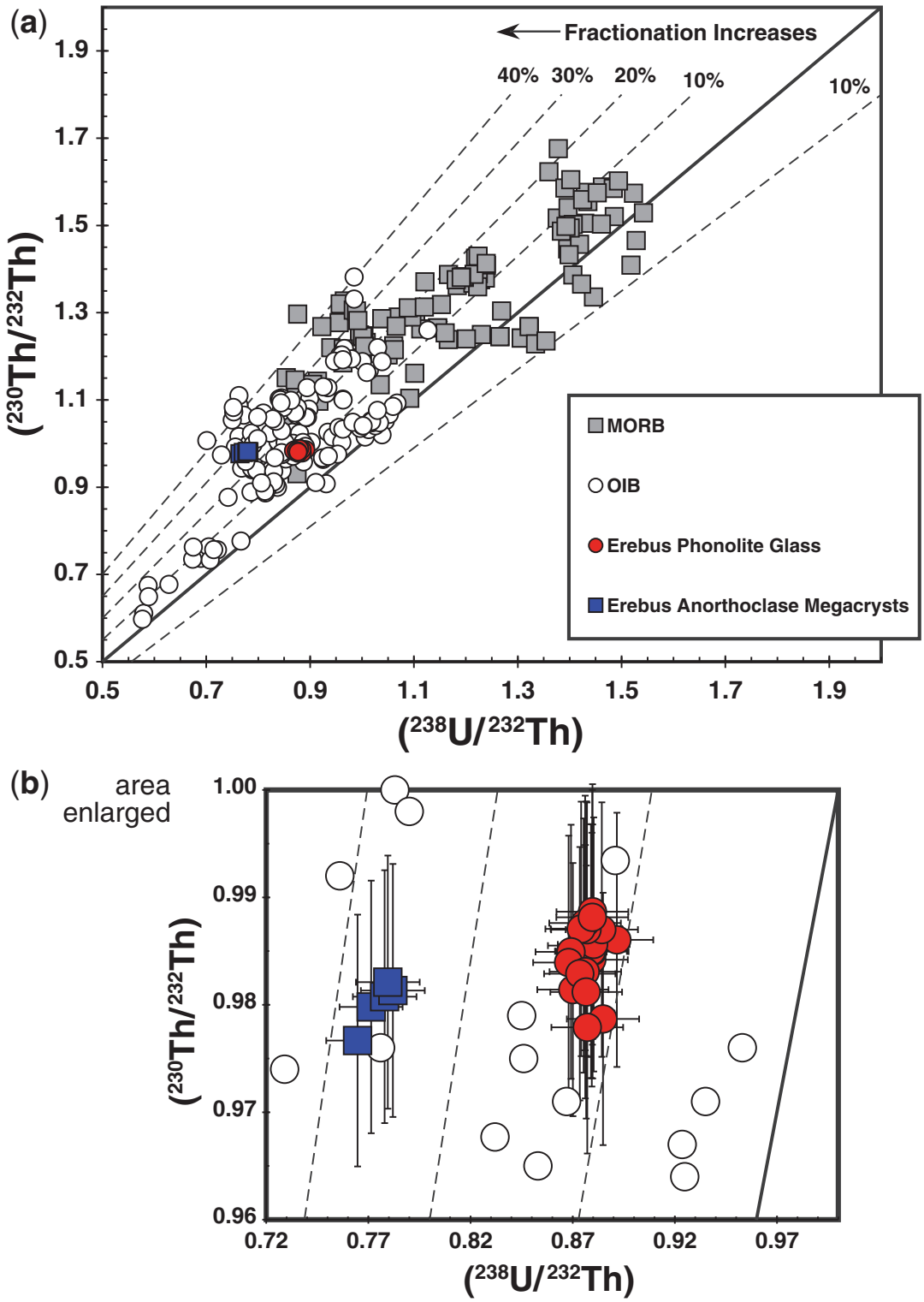

Fig. 3. (a) (^{230}Th/^{232}Th) vs (^{238}U/^{232}Th) isochron plot showing the Erebus samples compared with the global database for mid-ocean ridge basalt (MORB) and ocean island basalt (OIB). (b) Erebus data enlarged. The shift of anorthoclase megacrysts to lower U/Th exceeds what would be predicted from experimental uncertainties and is interpreted to be due to apatite inclusions (see text for discussion).

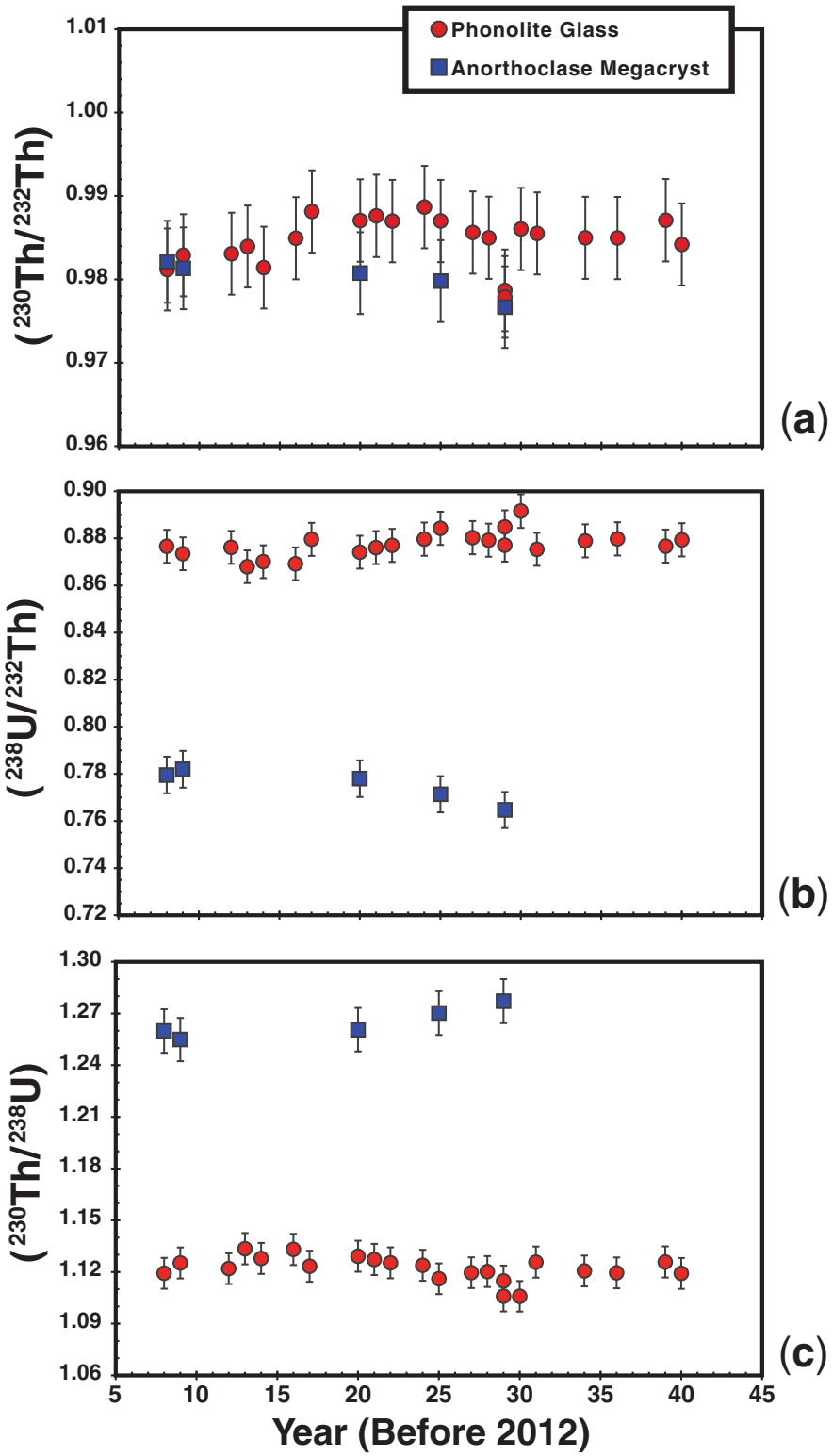

Fig. 4. Time-series data for (a) (^{230}Th/^{232}Th), (b) (^{238}U/^{232}Th), and (c) (^{230}Th/^{238}U) over the 34 year historical record from 1972 to 2005. Time is since 2012.

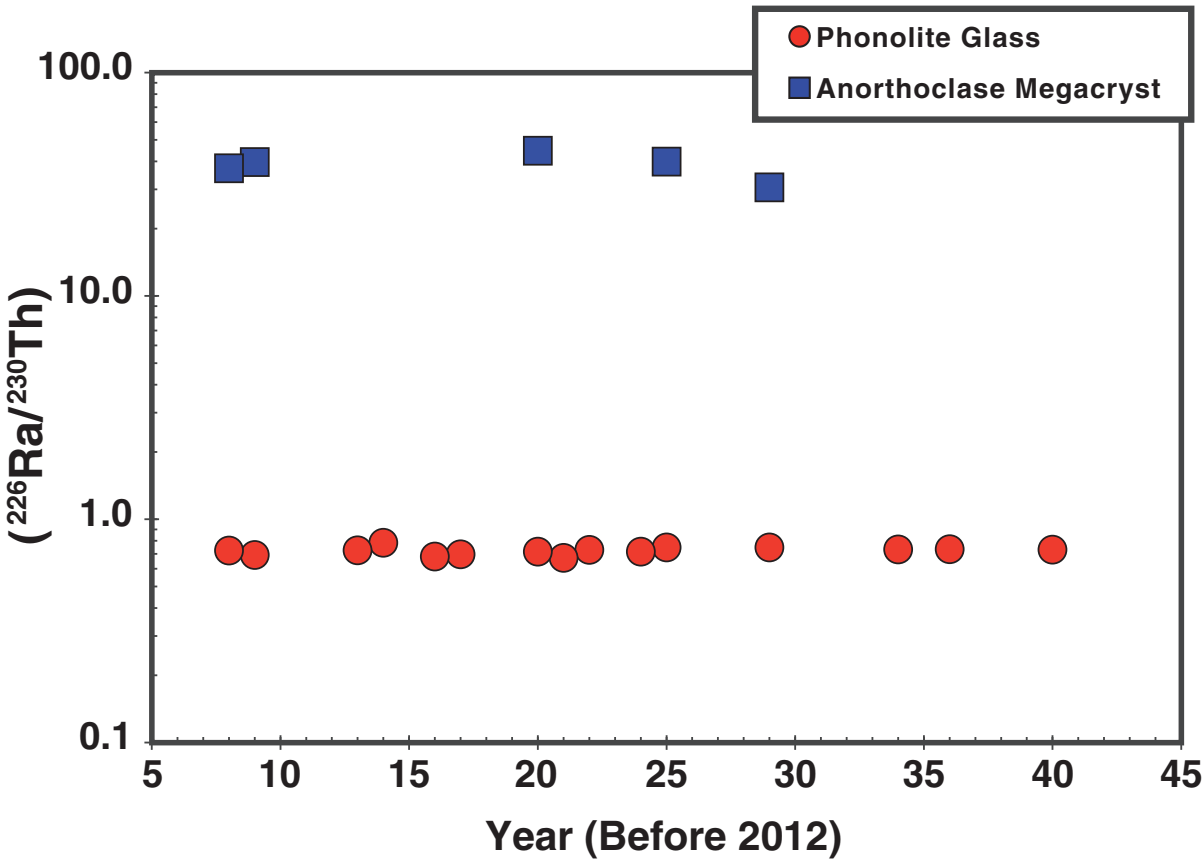

Fig. 5. Time-series data for (^{226}Ra/^{230}Th) over the 34 year historical record from 1972 to 2005. Time is since 2012.

during and prior to eruption, creating an initial ^{210}Po deficit relative to the ^{210}Pb grandparent (e.g. Gill *et al.*, 1985; Reagan *et al.*, 2006). In this sample, $(^{210}Po/^{210}Pb)_I = 0{\cdot}28$, and thus Po was not entirely degassed upon eruption.

^{232}Th decay series

^{232}Th–^{228}Ra–^{228}Th

As a proxy for ^{228}Ra ($t_{1/2} = 5{\cdot}77$ years), we measured ^{228}Ac and ^{208}Tl by gamma spectroscopy in 10 glass samples (Fig. 8; Table 2). The ^{228}Ac proxy assumes that (^{228}Ra) is in radioactive equilibrium with its daughter (^{228}Ac), which is a reasonable assumption given the extremely short half-life of ^{228}Ac ($t_{1/2} = 6{\cdot}13$ h). The ^{208}Tl proxy assumes that (^{228}Ra) is in radioactive equilibrium all the way down the chain to its distant granddaughter (^{208}Tl), which is also reasonable as the half-lives of these different nuclei range from less than 1 μs to 3·6 days. All samples have (^{228}Ac/^{232}Th) and (^{208}Tl/^{232}Th) in radioactive equilibrium to within 1σ counting uncertainties (Fig. 8), and thus, by inference, they are in equilibrium with respect to (^{228}Ra/^{232}Th).

The count rates were below detection limits for ^{228}Ac and ^{208}Tl gamma spectrometry of anorthoclase (Table 2). For the 2005 anorthoclase separate, (^{228}Ra/^{232}Th) was determined using ^{228}Th/^{232}Th measured by alpha spectroscopy as a proxy. The half-life of ^{228}Th is 1·9 years, so for this 3-year-old sample the (^{228}Ra/^{232}Th) inferred from (^{228}Th/^{232}Th) is a minimum estimate as the system had not attained full equilibrium.

^{235}U decay series

^{235}U–^{231}Pa

^{231}Pa ($t_{1/2} = 32\,757$ years) was measured on eight samples (1989, 1991, 1992, 1993, 1999, 2000, 2004, 2005). The WHOI (^{231}Pa/^{235}U) data range from 1·22 to 1·33, with an average of $1{\cdot}24 \pm 0{\cdot}04$ (1σ), whereas the Bristol laboratory found lower U and Pa concentrations and (^{231}Pa/^{235}U) ranging from 0·98 to 1·26. The higher value is similar to that measured at WHOI. This variability in the Bristol data and its deviation from the WHOI data is attributed to the Bristol samples being whole-rock aliquots containing significant, but variable amounts of anorthoclase and other crystalline phases. We note that because the Pa does not vary systematically with U and Th concentrations, it is likely that anorthoclase is not the only phase affecting the variability in (^{231}Pa/^{235}U) measurements.

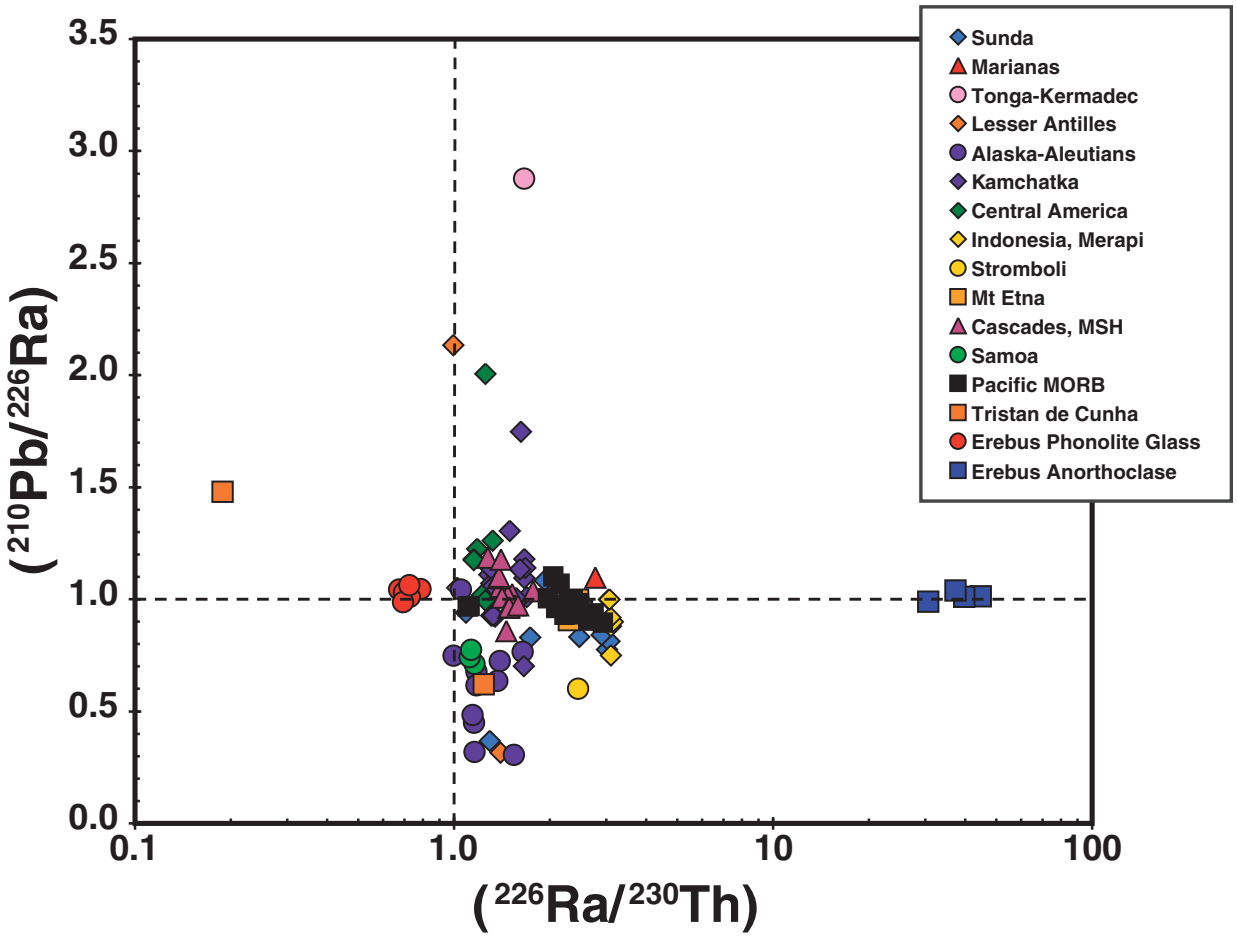

Fig. 6. (^{210}Pb/^{226}Ra) vs (^{226}Ra/^{230}Th) for Erebus samples compared with a global compilation. Data from Gauthier & Condomines (1999), Turner *et al.* (2004), Rubin *et al.* (2005), Reagan *et al.* (2006, 2008) and Berlo & Turner (2010).

^{231}Pa–^{227}Ac

^{227}Ac ($t_{1/2}$ = 21·77 years) was measured on two phonolite glass samples (1999 and 2004). In both samples (^{227}Ac/^{231}Pa) is unity within analytical uncertainty. The absence of ^{231}Pa–^{227}Ac disequilibria suggests that either no magmatic process, such as melting or crystallization, has chemically fractionated ^{231}Pa from ^{227}Ac or if they were chemically fractionated then this process occurred more than 100 years ago.

In situ analysis of anorthoclase and melt inclusions

Average Ba and Th concentrations in two 1984 (ER84-01 and ER84-04) and one 1988 (ER88-01) anorthoclase megacrysts are presented in Table 4 (see Appendix Table A1 for raw data). The Ba concentrations in melt inclusions measured by ion microprobe are highly variable, but overall comparable with the ID values obtained by MC-ICP-MS in this study. The Th concentrations measured by ion microprobe in the anorthoclase are significantly lower than those obtained on bulk mineral separates using ID-ICP-MS.

For the electron microprobe measurements, Pb and U concentrations in Erebus apatite were always below the detection limit of 100 and 40 ppm, respectively, whereas the Th concentration ranges from slightly above detection limit (40 ppm) up to around 100 ppm.

DISCUSSION

Phonolites ejected by the Strombolian activity of the Erebus lava lake have been sampled on an almost yearly basis from 1972 to 2005 (Figs 4, 5 and 8). This sample suite has allowed for comprehensive geochemical analysis (Kyle *et al.*, 1992; Caldwell & Kyle, 1994; Kelly *et al.*, 2008b; Sims *et al.*, 2008*a*) and provides a unique opportunity to constrain the temporal evolution of these highly differentiated lavas. These constraints are most robust with regard to the shallow, most differentiated part of the Erebus system because of the great petrological gap between the

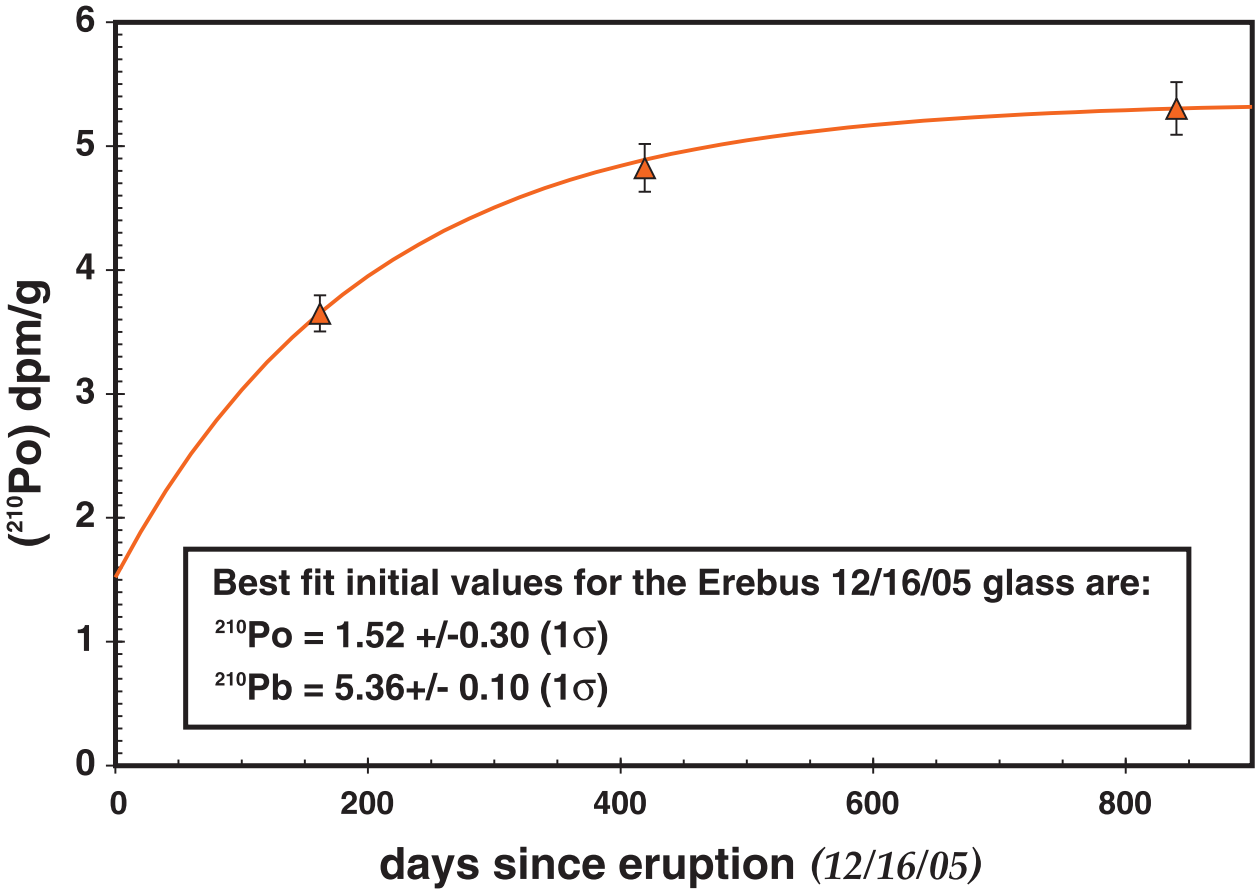

Fig. 7. (^{210}Po) measurements for the sample erupted on 16 December 2005 showing ingrowth curve from ^{210}Pb.

differentiated phonolites and their mantle-derived parental basanites.

Temporal variations in U-series

Anorthoclase and glass separates each have (^{230}Th/^{232}Th), (^{238}U/^{232}Th), (^{230}Th/^{238}U) and (^{226}Ra/^{230}Th) activity ratios that are uniform and normally distributed within analytical uncertainties. The one possible exception to this temporal uniformity is a bomb erupted in 1984 during a 4 month period of sustained Strombolian eruptions. Both ER 84501G and ER 84505G (which were replicated six times on separate powder aliquots) have lower (^{230}Th/^{232}Th) and skew the distribution slightly (Table 5). The average (^{230}Th/^{232}Th) for these two 1984 bombs, including replicates, is $0{\cdot}9767 \pm 0{\cdot}0045$ (2σ), whereas the average (^{230}Th/^{232}Th) for all the bombs from other years, including replicates, is $0{\cdot}9854 \pm 0{\cdot}0046$ (2σ). Admittedly, this difference is small (8·9 per mil) and overlaps at the 95% confidence level. However, in light of the fact that (1) 1984 was an exceptional year with larger and more frequent Strombolian eruptions (Kyle, 1986; Caldwell & Kyle, 1994) than previous and following years, and (2) the 1984 bombs have slightly lower ^{206}Pb/^{204}Pb and ^{208}Pb/^{204}Pb and higher ^{87}Sr/^{86}Sr (Sims *et al.*, 2008*a*), we consider this difference in (^{230}Th/^{232}Th) as possibly real. For the long-lived isotopes we hypothesized that this difference for the 1984 bombs reflected a change in the magma conduit resulting in assimilation of shallow-level trachytes (Sims *et al.*, 2008*a*).

Anorthoclase/phonolite glass partitioning

The (^{230}Th/^{238}U) and (^{226}Ra/^{230}Th) measurements of co-existing anorthoclase and phonolite glass provide a relative sense of U/Th and Th/Ra partitioning during anorthoclase crystallization. (^{230}Th/^{232}Th) is the same in both the anorthoclase and phonolite glass, whereas (^{238}U/^{232}Th) is fractionated (lower in the anorthoclase), suggesting that Th is more compatible than U. (^{226}Ra/^{230}Th) is much greater in the anorthoclase than in the phonolite glass, indicating that Ra is more compatible than Th. The relative partitioning of Ra and Pb cannot be determined from (^{210}Pb/^{226}Ra), as this activity ratio is unity (i.e. in radioactive equilibrium) in both phases.

Using our measured ^{238}U, ^{232}Th, ^{226}Ra and Ba concentrations for the phonolite glasses and anorthoclase separates (Table 1), we can calculate 'effective' anorthoclase/melt

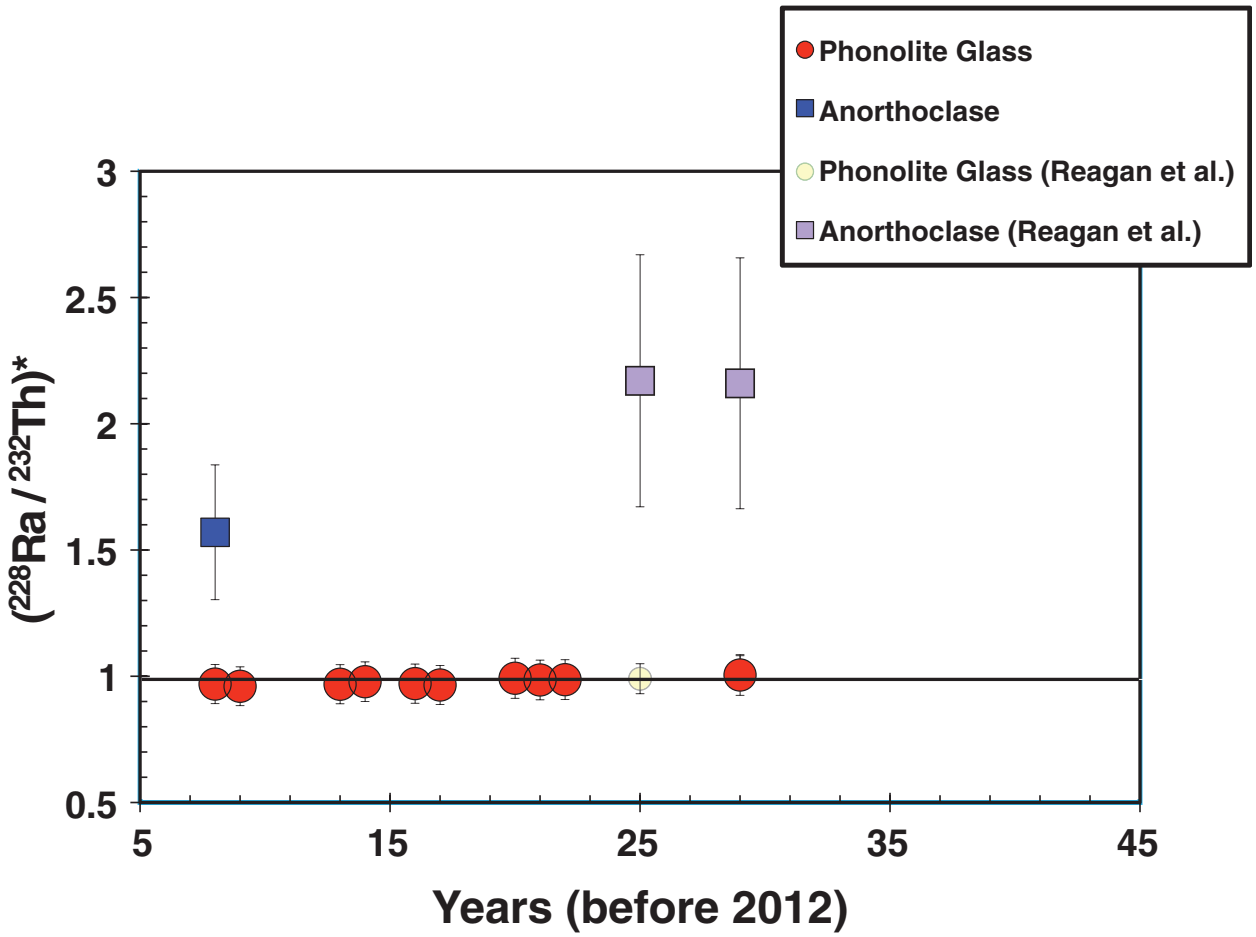

Fig. 8. Time-series data for ^{228}Ra over the 34 year historical record from 1972 to 2005. Time is since 2012. *(^{228}Ra/^{232}Th) was determined using ^{228}Th/^{232}Th measured by alpha spectroscopy as a proxy. The half-life of ^{228}Th is 1·9 years, so for this 2005 sample (measured in 2008) the (^{228}Ra/^{232}Th) inferred from (^{228}Th/^{232}Th) is a minimum value as the system had not yet attained full equilibrium. Reagan *et al.* (1992) data are shown for comparison.

partition coefficients for Th, U, Ra and Ba (Table 6). The calculated order of compatibility is $D_U < D_{Th} \ll D_{Ra} \ll D_{Ba}$. These calculated partition coefficients (D values) represent values averaged over the whole of several crystals (10 g) and are limited by the purity of the anorthoclase and phonolite glass separates. The observation that the D values are very different but relatively uniform for all five anorthoclase–glass pairs suggests that the separation methods were effective. D_{Ra} is determined from ^{226}Ra, which has been decaying (within the anorthoclase) and ingrowing (within the glass) toward an 'equilibrium' value with ^{230}Th over the lifetime of the crystal. Thus, the calculated D_{Ra} is a minimum value.

We can also calculate 'effective' anorthoclase/phonolite melt partition coefficients (Table 6) using our *in situ* Th and Ba measurements for anorthoclase and included melt. The *in situ* Ba concentrations show a large range of 'intra'-crystal variability reflecting both true compositional variations within the crystal and uncertainties in the measurement. This variance is in contrast to the bulk separates, which show rather limited 'inter'-crystal differences over five separate samples from different years. At the 1σ confidence level, the average D_{Ba} calculated from the *in situ* SIMS measurements overlaps the D_{Ba} calculated from the bulk anorthoclase. This similarity in the two different calculated values for D_{Ba} suggests that the 'bulk' anorthoclase and glass separates represent a homogenized average relatively clean from mutual cross-contamination in terms of their Ba (and by inference Ra) budget(s). The *in situ* Th concentrations of the melt inclusions measured by SIMS are also similar to the ID-ICP-MS measurements for the bulk glass separates. However, for the anorthoclase megacrysts, the *in situ* Th concentrations are much lower than the Th concentrations measured in the bulk separates. The resulting D_{Th} values calculated from the *in situ* measurements are lower than determined from the bulk separates.

The large difference in U/Th between the anorthoclase and phonolite glass exceeds the extent of elemental

Table 5: Mean, standard deviation, median, kurtosis and skewness of the distribution, and range of Erebus lava bombs, with and without the 1984 samples

	[Th] (μg g^{-1})	[U] (μg g^{-1})	Th/U	(^{238}U/^{232}Th)	[^{230}Th/^{232}Th]$_{atm}$ (ppm)	(^{230}Th/^{232}Th)
Phonolite glasses						
1984 bombs included						
n	22	22	22	22	22	22
Average	30·031	8·687	3·457	0·878	5·322	0·985
2σ SD	2·271	0·685	0·041	0·011	0·028	0·006
Median	30·162	8·701	3·459	0·877	5·322	0·985
Maximum	31·824	9·228	3·496	0·892	5·342	0·989
Minimum	26·771	7·677	3·403	0·868	5·284	0·978
Skewness	−0·843	−0·992	−0·458	0·509	−1·049	−0·940
Kurtosis	1·840	2·262	1·437	1·521	1·504	0·483
Without 1984 bombs						
n	20	20	20	20	20	20
Average	30·110	8·707	3·459	0·877	5·324	0·985
2σ SD	2·326	0·708	0·041	0·011	0·023	0·004
Median	30·459	8·792	3·460	0·877	5·323	0·985
Maximum	31·824	9·228	3·496	0·892	5·342	0·989
Minimum	26·771	7·677	3·403	0·868	5·301	0·981
Skewness	−1·064	−1·168	−0·574	0·630	−0·418	−0·418
Kurtosis	2·254	2·482	1·941	2·056	−0·417	−0·417
Anorthoclase megacrysts						
n	5	5	5	5	5	5
Average	0·238	0·061	3·915	0·775	5·296	0·980
2σ SD	0·035	0·009	0·036	0·007	0·011	0·002

	(^{230}Th/^{238}U)	[^{226}Ra] (fg g^{-1})	(^{226}Ra/^{230}Th)	Ba ICP-MS* (μg g^{-1})	Ba-ID (μg g^{-1})
Phonolite glasses					
1984 bombs included					
n	22	15	15	20	5
Average	1·122	2361·2	0·72	446·95	494·10
2σ SD	0·014	166·3	0·06	48·34	29·78
Median	1·123	2324·1	0·73	451·5	495·64
Maximum	1·134	2559·9	0·78	499	512·4
Minimum	1·106	2291·6	0·67	404	473·49
Skewness	−0·737	1·3	0·13	−0·234	−0·31
Kurtosis	0·866	0·8	0·57	0·344	−0·36
Without 1984 bombs					
n	20	14	14	18	4
Average	1·123	2359·3	0·72	445·5	499·25
2σ SD	0·012	172·0	0·06	50·12	21·79
Median	1·124	2315·2	0·72	447	499·01
Maximum	1·134	2559·9	0·78	499	512·4
Minimum	1·106	2291·6	0·67	404	486·58
Skewness	−0·780	1·4	0·30	−0·069	0·115
Kurtosis	2·169	0·8	0·88	0·219	−0·280
Anorthoclase megacrysts					
n	5	5	5		5
Average	1·265	982·2	38·46		2401·8
2σ SD	0·009	75·0	5·13		106·6

Table 6: Calculated anorthoclase/phonolite glass partition coefficients for U, Th, Ra and Ba based on isotope dilution measurements (Table 1) and for Th and Ba based on in situ measurements (Table 4)

	D_{Th}	D_U	D_{Ra}	D_{Ba}
Bulk analysis of separated phases				
Average	0·0080	0·0071	0·42	4·86
SD (1σ)	0·0013	0·0011	0·04	0·25
In situ *measurements*				
Average	0·0032			4·37
SD (1σ)	0·0022			0·19

The average values are calculated from the individual effective anorthoclase/phonolite glass partition coefficients.

fractionation predicted for either alkali or plagioclase feldspar crystallization (Blundy & Wood, 2003). Because the Th concentrations for anorthoclase measured *in situ* are much lower than measured in the bulk 'anorthoclase' separates we hypothesize that mineral separation failed to fully remove small mineral inclusions, such as apatite, from the anorthoclase and that these accessory mineral inclusions are influencing Th/U fractionation. The Erebus anorthoclase crystals contain abundant mineral inclusions of pyroxene, apatite, titanomagnetite, olivine and pyrrhotite trapped along apparent growth zones in the anorthoclase crystals (Fig. 2). Detailed BSE imaging of a set of 23 variably sized anorthoclase crystals indicates that pyroxene is the most abundant included phase, and also is the largest of the included phases, with sizes commonly up to 1 mm or greater. Apatite inclusions are also present in every crystal studied, and apatite is estimated to be the second most abundant included crystal. Many apatite crystals are small (of the order of 100 μm), but some larger crystals (up to 1 mm in length) are observed. Using image processing of Ca X-ray maps, the determined surface abundance of apatite ranges from 0·03 to 0·38% with an average of 0·14%. Most of the values for surface per cent of apatite exposed fall in a relatively small range between 0·07 and 0·15%. Accessory minerals, such as apatite, contain large amounts of U and Th (this work; Dawson & Hinton, 2003). Apatite/silicate melt U and Th partitioning experiments by Prowatke & Klemme (2006) showed that D_{Th} and D_U range from nearly equal to $D_{Th} > D_U$ (with D_{Th}/D_U ranging from 0·7 to 12·78). Our electron probe measurements of Erebus apatite also suggest that Th is more compatible than U in apatite, the Th in the apatite ranging from 40 to 100 ppm, whereas U was below the detection limit (40 ppm). Given the extent and size of apatite in the Erebus anorthoclase and its potential to fractionate U from Th we suggest that our mineral separation methods did not adequately remove the apatite from the anorthoclase and that these small apatite inclusions lowered the ($^{238}U/^{232}Th$) of the anorthoclase crystals. Thus, for anorthoclase–phonolite melt partitioning the D_{Th} determined from the *in situ* measurements is preferred over the D_{Th} determined from measurements of bulk anorthoclase and glass separates.

The complementary ($^{226}Ra/^{230}Th$) in the anorthoclase and phonolite glass provides strong evidence that anorthoclase crystallization chemically fractionates Ra from Th. Based on measured concentrations we calculate $D_{Ba} \sim 4·5$ (i.e compatible), $D_{Th}/D_{Ba} \sim 7e-4$ and $D_{Ra}/D_{Ba} \sim 0·1$. The observation that Ra and Ba are much more compatible than Th during feldspar crystallization is predicted theoretically (both Ra and Ba are alkali earths), and is consistent with partitioning experiments (Miller *et al.*, 2007; Fabbrizio *et al.*, 2009) and other measurements (Volpe & Hammond, 1991; Reagan *et al.*, 1992; Cooper *et al.*, 2001, 2003; Cooper & Reid, 2003; Zellmer *et al.*, 2008; Cooper, 2009; Rubin & Zellmer, 2009). Our value for D_{Ra}/D_{Ba} of ~0·1 is a lower limit (because of potential ^{226}Ra decay) and has important implications for using Ba as a stable proxy for Ra when evaluating the time scales of magma evolution and anorthoclase growth. Previous work on Erebus samples (Reagan *et al.*, 1992) assumed $D_{Ra}/D_{Ba} = 1$ during anorthoclase crystallization. However, Ba^{2+} and Ra^{2+} have different ionic radii (1·42 Å and 1·48 Å, respectively) in VIII-fold coordination (Blundy & Wood, 2003) and both theoretical predictions and experimental evidence indicate that D_{Ra}/D_{Ba} is significantly less than one during plagioclase and alkaline feldspar crystallization (Miller *et al.*, 2007; Fabbrizio *et al.* 2009). Because of the unusual composition of Erebus anorthoclase (An_{16} $Ab_{64·5}$ $Or_{18·7}$), the absolute and relative compatibilities of Ba and Ra are not easily predicted from theoretical models of elastic strain moduli. These models are for the end-member plagioclase or alkali feldspar series and assume single substitution, whereas during anorthoclase crystallization Ba and Ra partitioning would probably involve a coupled substitution. Nevertheless, using the parameterizations of, for example, Blundy & Wood (2003), for an alkali feldspar with an orthoclase composition of Or_{18}, D_{Ba} is predicted to be ~6·3 and D_{Ra}/D_{Ba} ~0·2, whereas for plagioclase with An_{17} (at ~1000°C) D_{Ba} is predicted to be ~1·4 and D_{Ra}/D_{Ba} ~0·22. These values are similar to those calculated by Fabbrizio *et al.* (2009), who used an orthoclase composition of Or_{19} and a temperature of 1000°C to calculate a D_{Ra}/D_{Ba} of 0·29. These predictions are qualitatively consistent with our measured results, which indicate that during anorthoclase crystallization Ba is highly compatible and D_{Ra}/D_{Ba} is between 0·1 and one, with the partitioning ratio probably being closer to 0·1.

Crystal growth rates and the time scales of magma differentiation

Our measurements of ^{238}U–^{230}Th, ^{230}Th–^{226}Ra, ^{226}Ra–^{210}Pb and ^{232}Th–^{228}Ra–^{228}Th disequilibria provide four salient observations pertinent to determining anorthoclase crystal growth rates and magma residence times in the shallow Erebus system.

(1) On a ($^{230}Th/^{232}Th$) vs ($^{238}U/^{232}Th$) isochron diagram both the anorthoclase and phonolite glass show significant ($^{230}Th/^{238}U$) disequilibria and cluster tightly in two distinct groups forming horizontal two-point isochrons (Fig. 3).
(2) On a (^{226}Ra)/Ba vs (^{230}Th)/Ba isochron diagram, the anorthoclase and glass lie on opposite sides of the 'equiline' forming steeply inclined two-point isochrons (Fig. 9).
(3) ($^{210}Pb/^{226}Ra$) values are within error of equilibrium for both the anorthoclase and phonolite glass (Fig. 6).
(4) ($^{228}Ra/^{232}Th$) values are within error of equilibrium in the phonolite glasses, but ($^{228}Ra/^{232}Th$) is >1 for the anorthoclase (Fig. 8).

Instantaneous crystal fractionation with a magma residence time of 10^2–10^3 years is consistent with the first three of these four constraints. The ^{238}U–^{230}Th data form horizontal 'zero-age' isochrons having an age resolution of 5–10 ka; ^{230}Th–^{226}Ra data form inclined two-point isochrons giving ages of ~2500 years for $D_{Ra}/D_{Ba} = 1$, down to hundreds of years for $D_{Ra}/D_{Ba} = 0{\cdot}1$ (Fig. 10); and the anorthoclase and glass separates both have equilibrium ($^{226}Ra/^{210}Pb$) values suggesting that they are older than 100 years. The equilibrium ($^{227}Ac/^{231}Pa$) in the phonolite glasses is also consistent with a magma residence time greater than 100 years, but without measurements of these nuclides in the anorthoclase these data have no direct bearing on the time scales of anorthoclase crystallization.

That being said, however, the observation that ($^{228}Ra/^{232}Th$) significantly exceeds unity in several young (1984, 1988) anorthoclase separates (Reagan *et al.*, 1992, 2006; this study) is inconsistent with simple instantaneous crystal growth and requires some portion of the crystal to have grown less than 25 years prior to eruption. This is not surprising as numerous petrographic observations, *in situ* measurements, and determinations of crystal size distributions (e.g. Dunbar *et al.*, 1994; Sumner, 2007; Kelly *et al.*, 2008*b*) suggest that anorthoclase crystal growth was episodic and probably continued until eruption. Additionally, there are considerable data indicating that crystallization of magmas occurs over significant periods of time (tens to thousands of years) as heat is transferred away from the magma-wall–rock interface (see, e.g. Albarède, 1993; Charlier & Zellmer, 2000; Vazquez & Reid, 2002; Turner *et al.*, 2003; Hawksworth *et al.*, 2004; Zellmer & Clavero, 2006; Reagan *et al.*, 2008). In light of this understanding, it is essential to explicitly consider the time scales of magma differentiation processes in the context of the half-lives of the shorter-lived U and Th decay series nuclides (e.g. ^{226}Ra, ^{210}Pb, ^{210}Po, ^{222}Rn, ^{227}Ac, ^{228}Ra, ^{228}Th, etc.).

To account for all of the abundances of short-lived nuclides in the ^{238}U and ^{232}Th decay series in a manner consistent with our understanding of mineral abundances, partition coefficients, and geochemical variations in the Erebus system, we have developed a finite-element, continuous crystallization model (Figs 11–13). Although our initial model is similar in many respects to the continuous constant rate crystallization model presented by Snyder *et al.* (2004, 2007) for ^{238}U–^{230}Th–^{226}Ra, we have the distinctive added requirement to be able to explain all of the U and Th decay time-series fractionations, including the very short-lived ^{232}Th–^{228}Ra system.

The objective of our modeling is to reproduce all of the observed U and Th decay series disequilibria, as well as Th and Ba abundances in both the phonolite glass and the anorthoclase. As starting compositions we use a tephriphonolite ($SiO_2 = 55{\cdot}93$ wt%; $MgO = 1{\cdot}23$ wt%) with compositions near the inflection point in the 'Erebus lineage' (Kyle *et al.*, 1992; Kelly *et al.*, 2008*a*) that marks the change from plagioclase to anorthoclase crystallization, causing Ba to switch from being incompatible to compatible. Because of the complementary ($^{226}Ra/^{230}Th$) values in anorthoclase–glass pairs, we assume that the Erebus phonolitic magmatic system was closed and as the anorthoclase grew the residual melt or magma was effectively fractionated. The assumed crystallizing assemblage contains 90% anorthoclase, which is typical of Erebus whole phonolite bombs (Kyle *et al.*, 1992; Kelly *et al.*, 2008*b*). The fractionation extent per step was chosen to produce a best-fit model at ~10 000 iterations (Appendix B).

The finite-element technique utilized here allows for a variety of crystallization models to be explored, including closed-system continuous crystallization (Fig. 12), variable-rate crystallization, even dissolution, and dissolution and recrystallization. These methods can also model open systems with magma recharge (Appendix B, Fig. 13). Nevertheless, because potential variations in crystallization rates are essentially unconstrained in this system, our models assume a constant rate of crystal fractionation (i.e. $dF/dt = k$) and therefore an approximately constant volumetric growth rate of anorthoclase (Fig. 12). Actual crystal growth consistent with this model does not necessarily have to be constant. Indeed, crystal size distribution studies (Dunbar *et al.*, 1994) at Erebus suggest that the anorthoclases have undergone multiple episodes of growth and periods of resorption. Nevertheless, as long as the rates of the processes that control parameters such as magma cooling and degassing rates remain roughly

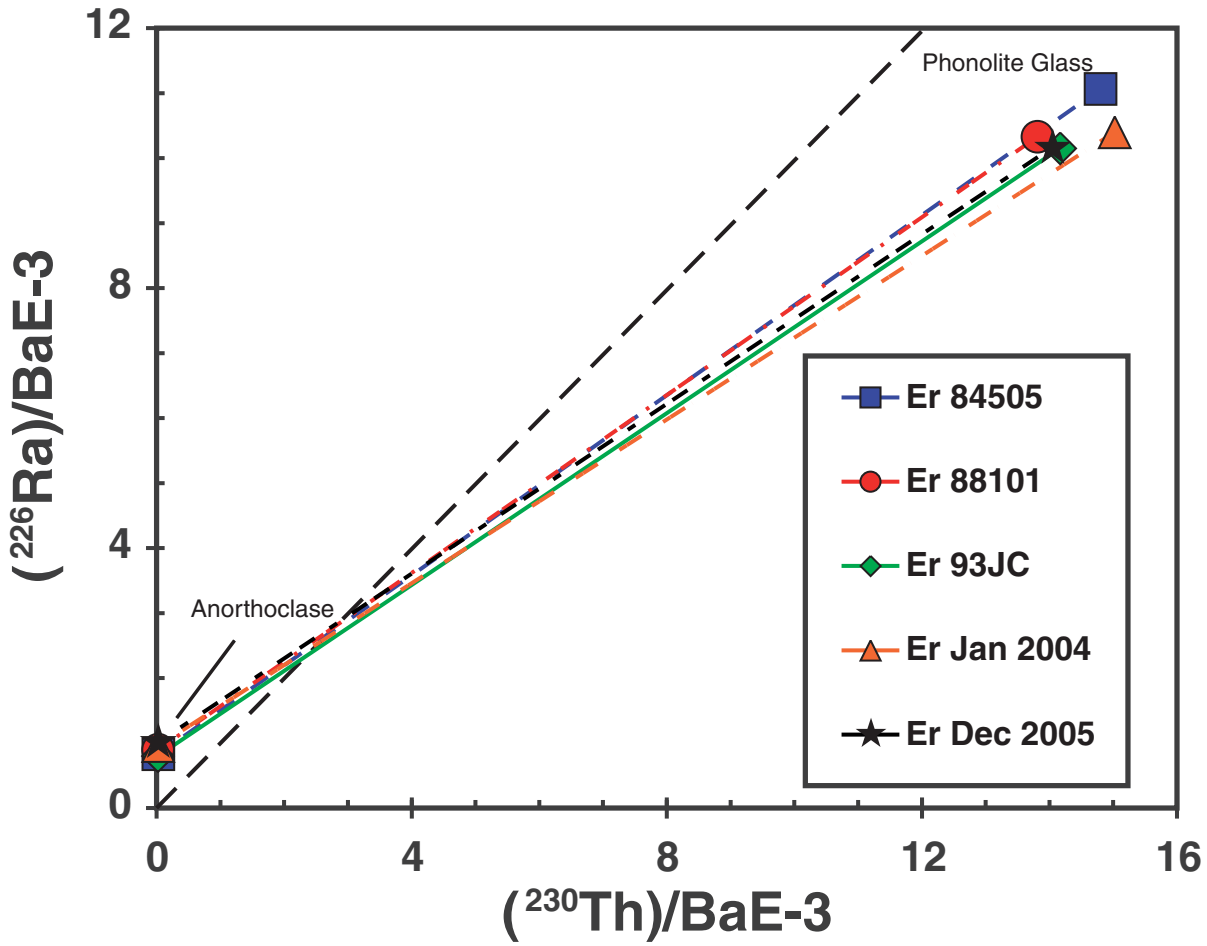

Fig. 9. Ra/Ba isochrons. ^{230}Th–^{226}Ra–Ba data for anorthoclase and glass separates plotted on a conventional Ba-normalized ^{230}Th–^{226}Ra isochron diagram

uniform, then the overall growth rate will be roughly constant.

Bulk partition coefficients for Ba and Th employed in these models are constrained by the *in situ* analyses, but as will be shown below, the effective partition coefficient for Th appears to differ slightly from measured values owing to the entrapment of melt and apatite during crystallization. D_{Ra} values are resolved in best-fit models by finding solutions that match (^{226}Ra/^{230}Th) and (^{228}Ra/^{232}Th) in the anorthoclase and glass separates. D_{Pb} values are not well constrained for these models because of a poor understanding of Pb concentrations in the starting magmas and the equilibrium (^{210}Pb/^{226}Ra) values measured in the young phonolites. We use bulk $D_{Pb} = 0{\cdot}2$, which is the value given for K-feldspar in trachyte by Larsen (1979), and is consistent with the positive correlations between Pb and other incompatible trace elements in differentiated alkaline lavas from Erebus (Kyle *et al.*, 1992; Kelly *et al.*, 2008*b*).

We first explored a variety of closed-system crystallization models (no recharge) to reproduce the compositions of Erebus anorthoclase and glass separates (Fig. 12). All the crystallization models using partition coefficients close to those measured did not fractionate Th and Ba to the level required. For example, the amount of crystallization required to reproduce the Th concentrations in the phonolite glasses removed too much Ba from the melt (Table 4). The Ba concentrations must have been maintained at higher levels than allowed for by anorthoclase crystallization, which implies that magma recharge was accompanying crystallization.

We then employed a numerical approach similar to the closed-system models, but in this model we allow magma recharge to accompany crystallization. Our initial open-system models utilized the measured partition coefficients from Table 6 for Th and Ba in anorthoclase, and assumed partition coefficients for both elements in other crystals in the crystallizing assemblage to be zero. To model both Th and Ba concentrations, magma recharge to crystallization rate ratios had to be above two. Whereas Th and Ba concentrations and the ratios between U-series nuclides can be

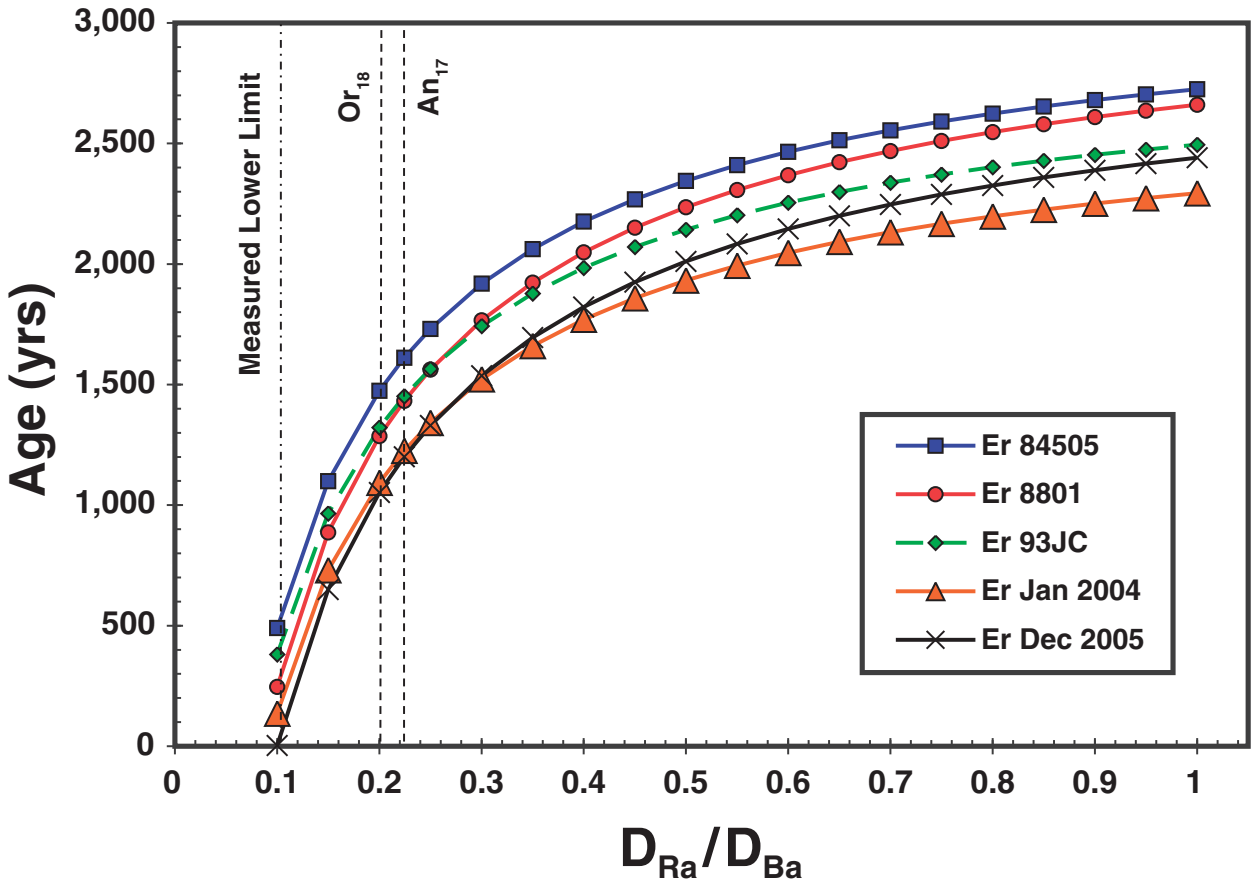

Fig. 10. Ra age vs D_{Ra}/D_{Ba} showing how the age of crystallization changes as a function of D_{Ra}/D_{Ba}. Calculated D_{Ra}/D_{Ba} values for Or_{18} and An_{17} are taken from Blundy & Wood (2003). The value of D_{Ra}/D_{Ba} of ~0·1 is a lower limit (because of potential ^{226}Ra decay).

reproduced utilizing the measured partition coefficients, the ($^{226}Ra/^{230}Th$) values were always higher in the models than in the glasses. This reflects the relatively low D_{Ra} required for modeling the ($^{226}Ra/^{230}Th$) values for the anorthoclase when the D_{Th} is within the range of measured values for the anorthoclase–glass pairs (<0·008). The models that fit the trace element and U-series data best utilize D_{Th} in anorthoclase of 0·012–0·016 (Table 6). An effective partition coefficient for Th in this range could result from the presence of 0·5–1% residual melt inclusion glass (and apatite) within the measured anorthoclase crystals. This level of melt entrapment would have little influence on the effective partition coefficients for compatible elements such as Ba. It should be noted that the D_{Ra}/D_{Ba} values of 0·2–0·24 in anorthoclase from these best-fit models are consistent with the theoretical feldspar values cited above, and having some residual glass during mineral purification is probable given that the anorthoclase megacrysts originally contained over 30% melt inclusions before purification.

As noted by O'Hara & Mathews (1981), trace elements eventually reach steady-state concentrations in magma chambers with constant recharge. The high recharge rates and degrees of crystallization modeled here are close to the values required for steady-state compositions to be attained, even for incompatible elements such as Th. Thus, the young anorthoclase phonolites from Erebus have major and trace element compositions that are close to those of a steady-state system.

The high recharge rates required by the best-fit models imply that the volume of phonolite in the shallow magma chamber and lava lake system at Erebus has been growing. This makes sense from a heat-balance point of view, as it explains how a lava lake and shallow magma reservoir can remain liquid (see Calkins *et al.*, 2008). Our modeled duration of reservoir growth is ~2000 years. This age coincides within error with the ages of the youngest two lavas from the flanks of Erebus (the Northwest and Upper Ice Tower Ridge flows; Harpel *et al.*, 2004). This permits speculation that the Erebus summit magma chamber system began to grow after these eruptive events and is at present amassing magma in advance of another significant lava eruption from a flank vent.

The open-system process required to produce Erebus phonolites and the calculated millennium-scale magma

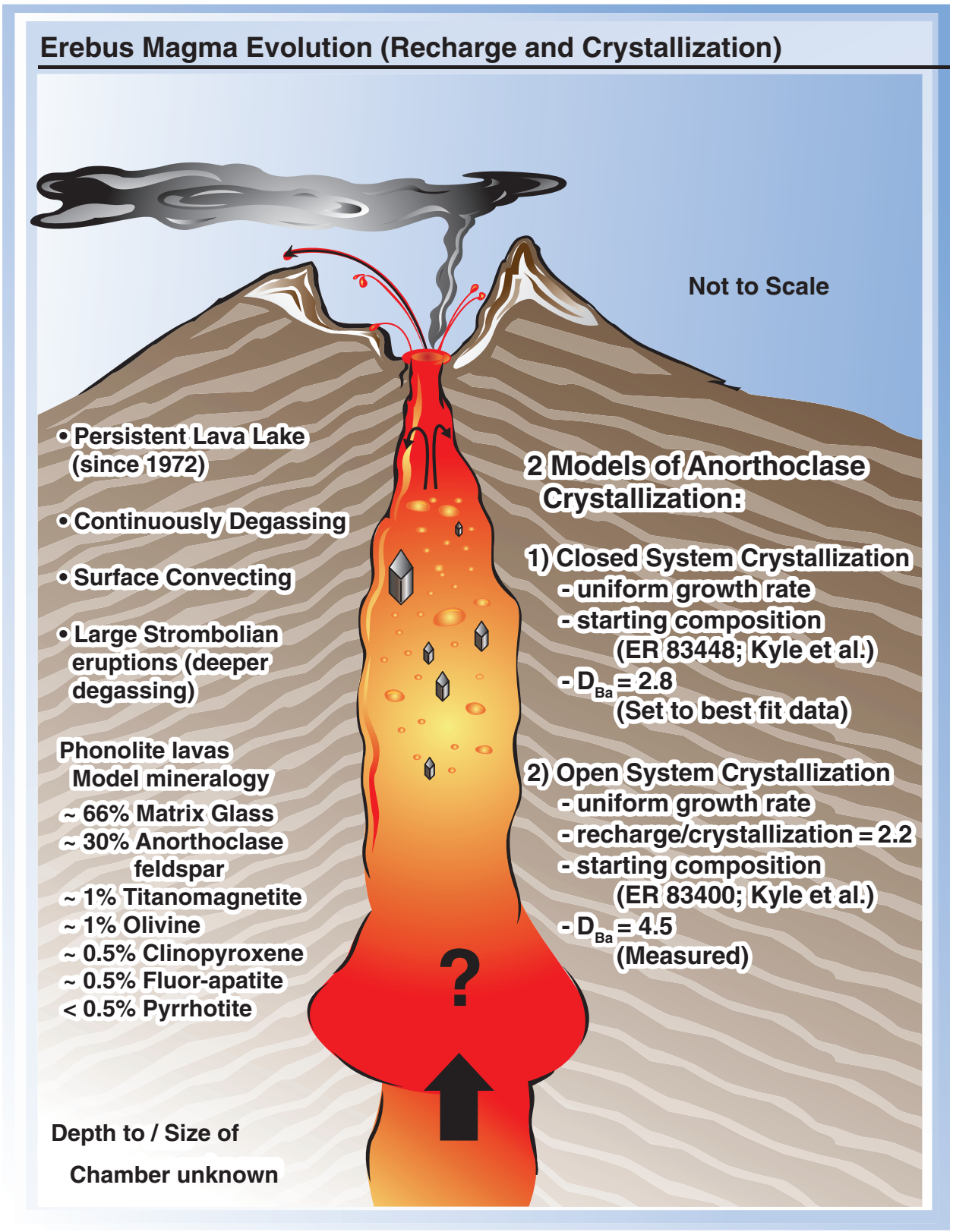

Fig. 11. Schematic illustration of the Erebus shallow magmatic system, detailing compositional constraints, model parameters and assumptions.

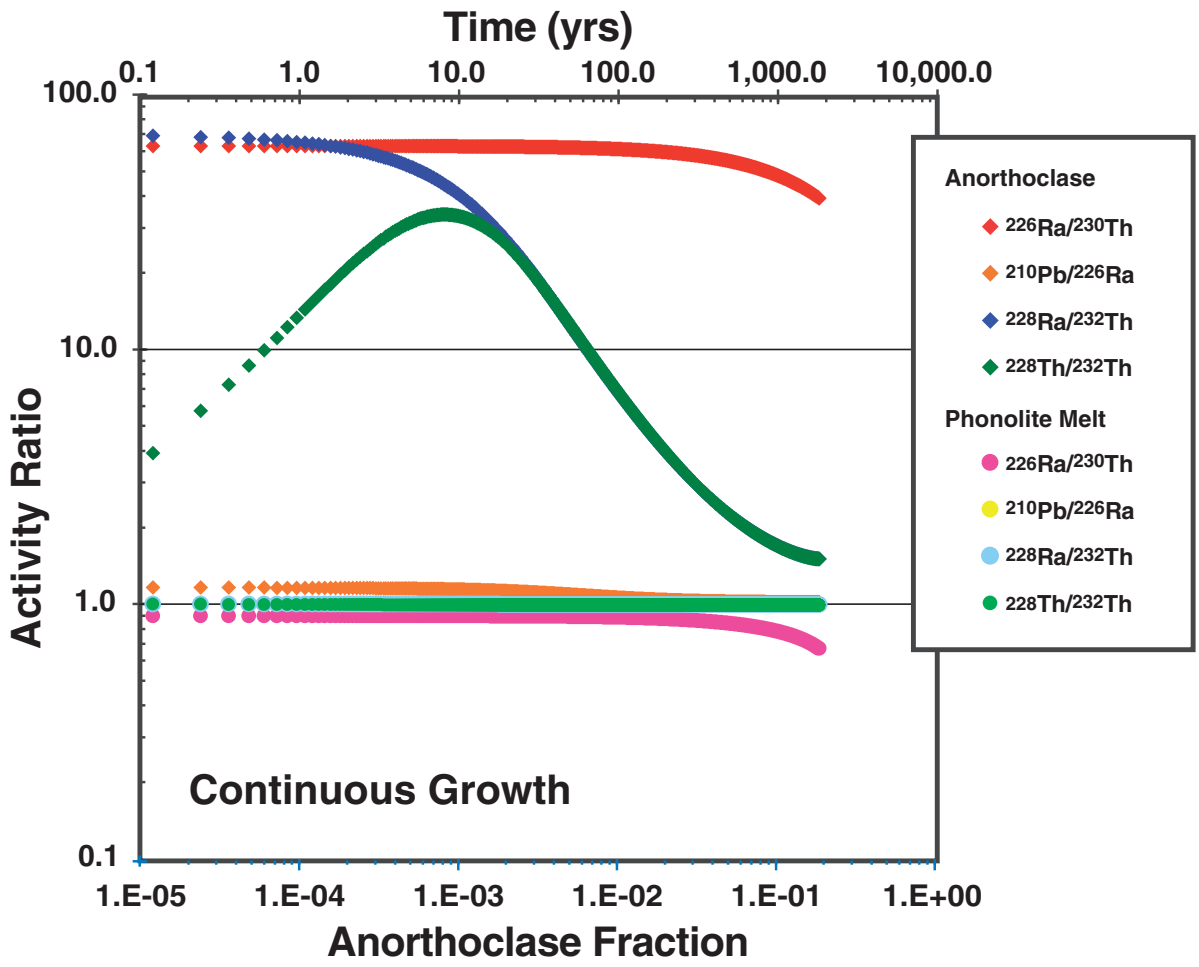

Fig. 12. Continuous closed-system crystallization model as described in the text.

accumulation time contrast significantly with the mode and time scale of production of the phonolite recently erupted subaqueously from the flanks of Nightingale Island near Tristan da Cunha (Reagan *et al.*, 2008). At Tristan da Cunha, the phonolite had trace element compositions consistent with its generation by simple crystal fractionation of more mafic parents. The Nightingale phonolite also had significant ^{210}Pb excesses over ^{226}Ra and small ^{228}Ra deficits with respect to ^{232}Th, implying that the crystal fractionation lasted one to three centuries. The contrast in short-lived radionuclide ratios between Nightingale and Erebus demonstrates the power of using these ratios in conjunction with other geochemical data to determine the mechanisms and time scales of magma differentiation. At Nightingale, the data are consistent with a small volume of isolated alkaline magma that rapidly fractionated to phonolite before eruption. In contrast, the compositions of Erebus phonolites suggest that the shallow magma body beneath its lava lakes is growing and has been doing so for about two millennia.

Ra–Th geochronometery

It has been debated how the ^{226}Ra–^{230}Th disequilibrium can be used as a geochronometer for petrological events in magmas (Cooper, 2009; Rubin & Zellmer, 2009). Rubin & Zellmer (2009) showed that if $D_{Ra} < D_{Th}$ in minerals (e.g. magnetite) in equilibrium with a melt, and the equilibrium process is terminated rapidly (e.g. by removal of the melt or rapid cooling), then the Ra–Ba isochron method (e.g. Fig. 9) can be used to mark the time since the equilibrium was maintained because the differences in D_{Ra} and D_{Ba} affect the calculated ages less than the precision of the technique. However, ages calculated using Ra–Ba isochrons and minerals with $D_{Ra} > D_{Th}$, such as the anorthoclase in Erebus phonolites, are erroneous because differences in D_{Ra} and D_{Ba} strongly affect the calculated ages (Fig. 10). In most cases, $D_{Ra} < D_{Ba}$ because of the greater size of Ra^{2+} relative to Ba^{2+}, which would lead to an overestimation of the age of any instantaneous event (Cooper *et al.*, 2001; Cooper & Reid, 2003; Cooper, 2009).

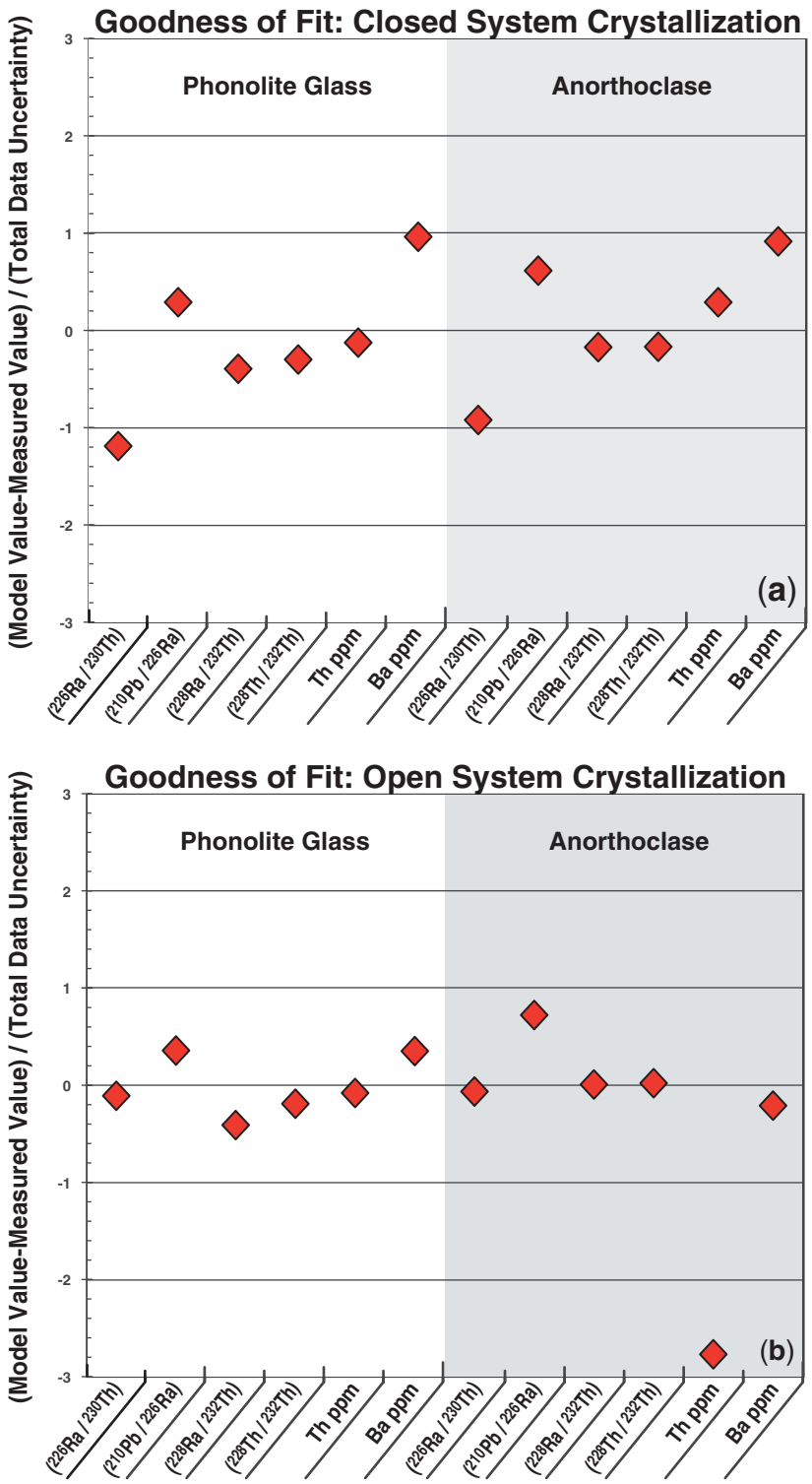

Fig. 13. (a) Goodness of fit of measured data to continuous closed-system crystallization model. It should be noted that the closed-system crystallization model (no recharge) cannot reproduce the compositions of Erebus anorthoclase and glass separates without setting the D_{Ba} anorthoclase/phonolite glass to a value of 2·8, indicating that the Ba concentrations must have been maintained at higher levels than allowed for by anorthoclase crystallization, implying that magma recharge was accompanying crystallization. (b) Goodness of fit of measured data to open-system crystallization model. Magma recharge to crystallization rate ratios set to a value of two. This uses the measured D_{Ba} anorthoclase/phonolite glass value of 4·5. For the crystals the Th misfit is interpreted to result from both residual apatite and glass that was not completely separated.

Another issue with using any isochron method on large and long-lived systems such as Erebus is that crystals can grow over significant amounts of time (e.g. Reagan *et al.*, 1992; this study) or can be recycled from older magmas (e.g. Pyle *et al.*, 1998; Reagan *et al.*, 2003; Sims *et al.*, 2007). Thus, bulk samples can contain crystals grown over a variety of time scales and conditions, and their chemical compositions represent integrated averages. To obtain quantitative geochronological information from Ra–Th disequilibria in this circumstance, a continuous long-duration model, such as the one used here, is required. We should note that the high recharge rates used in our open-system models extend the calculated magma accumulation time significantly farther than the time frame calculated by simple continuous crystal fractionation models.

Implications for the processes and time scales of magma degassing from $^{210}Pb/^{226}Ra$ and ^{210}Po

The measured equilibrium values for ($^{210}Pb/^{226}Ra$) and ($^{227}Ac/^{231}Pa$) and our open-system modeling for ($^{226}Ra/^{230}Th$) and ($^{228}Ra/^{232}Th$) suggest that the shallow magma residence time of the Erebus lavas is greater than 100 years. However, given that the Erebus lava lake is continuously degassing, both by quiescent emissions and Strombolian eruptions, the observation that ^{210}Pb is in equilibrium with ^{226}Ra (Fig. 8) is rather surprising. One would expect that removal of ^{222}Rn, a noble gas that lies between ^{226}Ra and ^{210}Pb, by magma degassing would have a significant impact on the ($^{210}Pb/^{226}Ra$) of the magma (see, e.g. Gauthier *et al.*, 2000; Berlo *et al.*, 2010; Reagan *et al.*, 2006; Kayzer *et al.*, 2009). Devolatilization generally has a negligible effect on the concentrations of ^{210}Pb or ^{226}Ra themselves, as Ra is not volatile, and only about 1% of Pb typically degasses from magmas (Lambert *et al.*, 1976; Rubin, 1997; Gauthier *et al.*, 2000). In contrast, Rn strongly partitions into the gas phase from magma (Sato & Sato, 1977; Sato *et al.*, 1980; Gill *et al.*, 1985; Sato, 2003; Sims & Gauthier, 2007). So, if magma degassing endures for years to decades, ($^{210}Pb/^{226}Ra$) values are lowered as a function of the half-life of ^{210}Pb and the ^{222}Rn degassing efficiency (Gauthier & Condomines, 1999). Similarly, if ^{222}Rn concentrates in the gas phase of a magma that has stalled somewhere, then ^{210}Pb generated by decay of ^{222}Rn can lead to a ^{210}Pb excess in the magma (e.g. Turner *et al.*, 2004; Berlo *et al.*, 2010; Reagan *et al.*, 2006; Kayzar *et al.*, 2009). However, it should be noted that tens to thousands of times as much magma must degas ^{222}Rn compared with the amount of magma that collects it because of the large differences in the half-lives of ^{222}Rn (3·8 days) and ^{210}Pb (22 years) (Reagan *et al.*, 2006; Kayzar *et al.*, 2009; Condomines *et al.*, 2010).

Given the observed persistent degassing of the Erebus lava lake (both quiescent and Strombolian), four scenarios can explain the measured ($^{210}Pb/^{226}Ra$) of unity in the young, known age Erebus phonolite bombs, as follows.

Hypothesis 1: ^{222}Rn is soluble in the Erebus phonolite melt and thus is not degassing from the magma. We consider this 'soluble ^{222}Rn scenario' highly unlikely as Rn is a 'noble gas' and therefore should not be soluble in the Erebus phonolite melt. Although concentrations of ^{222}Rn are too low to become saturated in the phonolite magma and produce a separate gas phase, it is generally assumed that ^{222}Rn degassing is governed by Henry's law partitioning of ^{222}Rn between magma and a gas phase resulting from saturation of the major volatile species H_2O, CO_2, and SO_2 (see, e.g. Gauthier & Condomines, 1999). H_2O, CO_2, and SO_2 are significantly degassing from the Erebus lava lake (Oppenheimer and Kyle, 2008; Oppenheimer *et al.*, 2009; Sweeney *et al.*, 2008) and thus a 'soluble ^{222}Rn scenario' would require the chemical behavior of the ^{222}Rn to be in marked contrast to that of the other gaseous species H_2O, CO_2, and SO_2. In addition, as will be discussed below, ^{210}Po has been degassed relative to ^{210}Pb, suggesting that the volatile, short-lived radionuclides are also being degassed.

Hypothesis 2: Mixing occurs between a surface magma, which has ($^{210}Pb/^{226}Ra$) < 1 from continuous degassing of ^{222}Rn, with a deep magma that has ($^{210}Pb/^{226}Ra$) > 1 from continuous ^{222}Rn accumulation. It is not possible to rule out this scenario, as the lava lake is convecting and in continuous motion, suggesting stirring of the system at the shallowest levels. Nonetheless, the perfect mass balance required to produce magma with ($^{210}Pb/^{226}Ra$) = 1 in all samples seems fortuitous.

Hypothesis 3: The anorthoclase-rich phonolite circulating in the upper part of the magmatic system is made of old, degassed magma that is not communicating with gas emissions that are coming from deeper parts of the magma chamber. This old, degassed magma hypothesis is also consistent with the observation that some melt inclusions in anorthoclase are highly degassed compared with those in olivines from parental basanites from around the flanks (Oppenheimer *et al.*, 2011). That said, there is clear persistent degassing of the Erebus lake and this degassing is hypothesized, based on Fourier transform infrared (FTIR) spectroscopic measurements, to have three components: (1) a passively emitted water-rich gas exolved near the lake surface when magma episodically enters the lake (mass CO_2/H_2O ~0·1); (2) a passively emitted deeper-sourced gas that percolates though a permeable magma-filled conduit (mass CO_2/H_2O ~1·8) (Oppenheimer *et al.*, 2009); (3) a deeper-sourced CO_2-rich gas (mass CO_2/H_2O ~4·3) observed during Strombolian eruptions (Oppenheimer *et al.*, 2011). For this third hypothesis to be correct, the gas sourced from deeper in the system would need to ascend without interacting with the shallow magma system.

Hypothesis 4: Internal redistribution of radon occurs between a deep degassing magma and a shallow previously degassed magma. In this 'internal radon redistribution' scenario degassing is occurring by two distinct processes: (1) weak shallow degassing from the lava lake; (2) more intense degassing from deeper levels. Melt inclusions in some anorthoclase crystals (Oppenheimer *et al.*, 2011) suggest that some lava lake phonolite is extensively degassed and thus could have a $(^{210}Pb)/(^{226}Ra)$ activity ratio significantly lower than one. If deeper degassing events, which are contributing significantly to the Erebus gas (CO_2) flux, supply radon to the shallowest level where it could decay and produce ^{210}Pb atoms, then this would counterbalance the ^{210}Pb loss owing to shallow ^{222}Rn degassing. Essentially, in this scenario the ^{222}Rn flux into the bottom of a shallow reservoir is equal to the ^{222}Rn flux out of the magma system.

Relevant to degassing at Erebus is the observation that a lava bomb erupted on 16 December 2005, has ^{210}Po not completely degassed from the lava at the time of eruption (Fig. 7). Incomplete degassing of ^{210}Po is atypical for subaerially erupted lavas (e.g. Gill *et al.*, 1985; Rubin *et al.*, 1994; Rubin, 1997; Reagan *et al.*, 2006, 2008). This incomplete degassing observed for the Erebus phonolite indicates that either the solubility of Po is higher than assumed in the Erebus phonolite (again unlikely given what we have seen in other volcanic systems), or that the average Erebus magma represented in the erupted lava bombs was on average degassed up to 80 days prior to eruption. Degassing could not have started two or more years before eruption or we would observe this in the $^{210}Pb/^{226}Ra$.

To quantitatively address the equilibrium $(^{210}Pb/^{226}Ra)$ (i.e. the effect of the intermediate volatile nuclide ^{222}Rn on this ratio) and the incomplete degassing of ^{210}Po, we have incorporated these volatile nuclides into our finite element model of magma evolution and anorthoclase crystallization discussed above. In this model, we assume that the intruding parental magma from depth was completely degassed and thus had activities of $^{210}Po = 0$ and $^{222}Rn = 0$ (^{210}Pb in the intruding magma can be set to almost any value from unity to zero without much effect on the model glass $^{210}Pb/^{226}Ra$). We set (1) the melt/gas partition coefficients of Rn and Po to zero, (2) the time steps to 7 days, which is about 5% of the half-life of ^{210}Po, and (3) ^{210}Po and ^{222}Rn to degass at 1·3% per day. Because of the short half-life of ^{222}Rn ($t_{1/2} = 3{\cdot}85$ days), ^{222}Rn ingrows rapidly, and thus the effect on ^{210}Pb (and $^{226}Ra/^{210}Pb$) is negligible. The $^{210}Po/^{210}Pb$ ratio, however, quickly moves to a steady-state value at 0·25, similar to the measured value (Fig. 7). Although this model fits the data well, it is probably not completely realistic as it assumes that the entire shallow magma chamber is stirred on a short enough time scale to keep $^{210}Po/^{210}Pb$ (and all other geochemical parameters) homogeneous throughout the chamber. Nevertheless, it shows that Erebus with its shallow stagnated magma does not lose all of its ^{210}Po all of the time. The model also implies that our samples resided only in the shallow chamber before being thrown out by the Strombolian explosions. This is in contrast to most lavas and tephra from other volcanoes that are tapped from deeper levels and degas over long paths to the surface (Reagan *et al.*, 2008).

U and Th decay series constraints on magma genesis and melt transport

In basaltic systems, it is well established that the longer-lived U-series isotopes (i.e. ^{230}Th, ^{226}Ra, ^{231}Pa) can provide important constraints on the processes and time scales of magma genesis, namely magma production rates, time scales of melt extraction and the lithology (garnet/cpx) of the mantle source (McKenzie, 1985; Speigelman & Elliott, 1993; Lundstrom *et al.*, 1995; Elliott, 1997; Sims *et al.*, 1995, 1999, 2002; Bourdon & Sims, 2003; Stracke *et al.*, 2006; Prytulak & Elliott, 2009; Waters *et al.*, 2011). However, in more evolved volcanic systems, such as at Erebus, shallow-level magmatic processes can overprint and thus obfuscate much of the information on the initial melting processes.

In the Erebus magma system, shallow crustal processes and time scales have clearly and significantly influenced the relative activities of ^{230}Th–^{226}Ra, ^{210}Pb–^{226}Ra, ^{210}Pb–^{210}Po, ^{232}Th–^{228}Ra and ^{235}Pa–^{227}Ac and, as a result, these parent–daughter nuclides cannot provide direct information on the time scales and nature of the initial melting processes. Even so, we argue that the U–Th isotope system can still provide constraints on the lithology (cpx/gt) and long-term nature of the Erebus mantle source.

With regard to the lithology (cpx/gt) of the Erebus mantle source, based on experimentally determined U and Th mineral–melt partition coefficients the large ^{238}U–^{230}Th disequilibria of the Erebus phonolites indicate that melting began deep and most probably in the presence of garnet (Beattie *et al.*, 1993a, b; LaTourrette *et al.*, 1993; Landwehr *et al.*, 2001; Elkins *et al.*, 2008). The $(^{230}Th/^{238}U)$ disequilibria measured in these phonolites are minimum values, as magma residence time would decrease the $(^{230}Th/^{232}Th)$ of the lava and apatite fractionation would increase its $(^{238}U/^{232}Th)$, which in both instances would decrease the $(^{230}Th/^{238}U)$ of the lava. Our modeling of the anorthoclase crystallization ages and magma residence times suggests that magma residence times in the upper part of the Erebus magma system are short relative to the half-life of ^{230}Th; as such, the decrease in $(^{230}Th/^{232}Th)$, because of ^{230}Th decay, will be insignificant compared with the analytical uncertainty. Although apatite fractionation appears to have lowered the $(^{238}U/^{232}Th)$ and attendant $(^{230}Th/^{238}U)$, it could not have produced the observed ^{238}U–^{230}Th disequilibria, for if it had, the Erebus lavas would be depleted in ^{230}Th relative to ^{238}U, rather than enriched as observed. Furthermore, because of (1) the small

amount of apatite in the Erebus lavas and phonolites, (2) the coherent behavior of U and Th as highly incompatible elements and (3) the lack of correlation between Th/U and P_2O_5 through the entire liquid line of descent seen in the Mt. Erebus lavas (basanite to phonolite), we conclude that it is unlikely that apatite has significantly altered the ($^{230}Th/^{238}U$) disequilibrium originally imparted by the melting process.

With regard to the mantle sources of the Erebus lavas, as noted by Sims & Hart (2006) and discussed in the background section above, the $^{230}Th/^{232}Th$ and U/Th of Erebus bombs are intermediate relative to other ocean island and mid-ocean ridge basalts, and form the end-member HIMU mantle component on plots of Pb isotopes versus ($^{230}Th/^{232}Th$) and U/Th. Although Erebus does not represent the end-member mantle component HIMU, there are no samples young enough for U–Th disequilibria studies from Mangaia–Tubaui (the HIMU end-member). Hence, for the U–Th isotope system, Erebus, by necessity, represents the best available end-member approximation for the HIMU source.

CONCLUSIONS

This is the first study in which all the relevant nuclides from the ^{238}U, ^{235}U, and ^{232}Th decay series have been measured in the lavas of a volcanic system. The contrasting chemistries and half-lives of these different nuclides have allowed us to investigate a variety of shallow magmatic processes over a wide range of time scales (from days to 10^5 years), thereby providing a better understanding of the rates and processes of magma differentiation than has been established in earlier studies. Furthermore, this work provides some perspective on the long-range hazard posed by the Erebus volcano.

The main conclusions from this study are as follows.

(1) U–Th–Ra disequilibria are uniform over 34 years of history. In the phonolite glass, from 1972 to 2005, ($^{238}U/^{232}Th$) and ($^{230}Th/^{232}Th$) are uniform, with one possible exception being the 1984 samples, which were erupted during a time of significantly increased Strombolian activity. ($^{226}Ra/^{230}Th$) is also uniform over the 34 year historical record. This uniformity suggests that the Erebus magma system, over the 34 year sample span, is in a state of dynamic equilibrium.

(2) For the Erebus lavas the equilibrium ($^{210}Pb/^{226}Ra$) and ($^{227}Ac/^{231}Pa$) suggest that the magma residence time is long compared with the half-lives of ^{210}Pb ($t_{1/2}=22{\cdot}6$ years) and ^{227}Ac ($t_{1/2}=21{\cdot}77$ years). However, the observation that ($^{228}Ra/^{230}Th$) ($t_{1/2}=5{\cdot}77$ years) is out of equilibrium in the anorthoclase suggests that the Erebus magmatic differentiation and crystallization processes are continuous and continuing. With this observation in mind we have developed an open-system, finite-element, continuous-crystallization model that incorporates ingrowth and decay of the different nuclides in the continuously growing anorthoclase crystals and associated phonolitic melt. Because we have measured Ba and Th concentrations in both the anorthoclase crystals and the melt we can constrain the anorthoclase/phonolite melt partitioning of Ba and Th and have found that the only way to replicate the observed Ba and Th concentrations and ^{238}U, ^{235}U and ^{232}Th decay series data is to incorporate magma recharge into the shallow system. To successfully model the present dataset the recharge rate has to exceed the crystallization rate, which implies that the shallow magma reservoir within Erebus is growing. This has important implications for hazard assessment. Our modeled duration of reservoir growth is ~2000 years, which coincides, within error, with the ages of the two youngest lavas from the flanks of Erebus (the Northwest and Upper Ice Tower Ridge flows; Harpel *et al.*, 2004). This observed coincidence indicates that the Erebus summit magma chamber system began to grow after these eruptive events and is at present amassing magma in advance of another significant lava eruption from a flank vent. An important cautionary implication of this modeling is that when the time scale of crystallization is comparable with the half-life of the daughter nuclide of interest, the simple isochron techniques typically used in most U-series studies can provide erroneous ages.

(3) ($^{210}Pb/^{226}Ra$) is in equilibrium despite the observed persistent degassing of the Erebus lava lake. This observation requires that either (1) ^{222}Rn is soluble in the Erebus phonolite melt and thus is not degassing from the magma, (2) mixing is taking place between a surface magma, which has ($^{210}Pb/^{226}Ra$) < 1 from continuous degassing of ^{222}Rn, and a deep magma that has ($^{210}Pb/^{226}Ra$) > 1 from continuous ^{222}Rn accumulation, (3) the anorthoclase-rich phonolite circulating in the upper part of the magmatic system and made of old, degassed magma is not communicating with gas emissions coming from deeper parts of the magma chamber, or (4) internal redistribution of radon is occurring between a deep degassing magma and a shallow previously degassed magma. The observed degassing of the Erebus lava has also partially removed ^{210}Po from the magma. As a result, we prefer the fourth model, in which the flux of the intermediate ^{222}Rn into the shallow system equals the flux of ^{222}Rn degassing out of the system.

(4) Although shallow-level magmatic processes at Erebus have obfuscated much of the information on the initial melting processes, the significant and uniform ^{230}Th excesses measured in the Erebus phonolites suggest that the parental basanites had residual garnet in their source.

(5) Finally, Erebus lavas form the end-member HIMU mantle component on plots of Pb isotopes versus ($^{230}Th/^{232}Th$) and U/Th.

ACKNOWLEDGEMENTS

Field work has been greatly facilitated by NSF-directed civilian contractors Raytheon Polar Services Company. Special thanks go to the helicopter crews from PHI and Helicopters New Zealand. Reviews by Georg Zellmer, John Hora and Ken Rubin, and editorial handling by Simon Turner are gratefully acknowledged.

FUNDING

This work was supported by NSF grant OPP-0126269 to K.W.W.S. and grants OPP-0125744 and ANT-0838817 to P.R.K., and French Institut National des Sciences de l'Univers and Agence Nationale de la Recherche grants (M&Ms) to J.B.-T. Fieldwork at Erebus volcano and operation of the Mount Erebus Volcano Observatory (erebus.nmt.edu) was supported by the Office of Polar Programs, NSF.

REFERENCES

Albarède, F. (1993). Residence time analysis of geochemical fluctuations in volcanic series. *Geochimica et Cosmochimica Acta* **57**, 615–621.

Ball, L. A., Sims, K. W. W. & Schwieters, J. (2008). Measurement of $^{234}U/^{238}U$ and $^{230}Th/^{232}Th$ in volcanic rocks using the Neptune PIMMS. *Journal of Analytical Atomic Spectrometry* **23**, 173–180, doi:10.1039/b703193a.

Bannister, S., Snieder, R. K. & Passier, M. L. (2000). Shear-wave velocities under the Transantarctic Mountains and Terror Rift from surface wave inversion. *Geophysical Research Letters* **27**, 281–284.

Beattie, P. (1993*a*). Uranium–thorium disequilibria and partitioning on melting of garnet peridotite. *Nature* **363**, 63–65.

Beattie, P. (1993*b*). The generation of uranium series disequilibria by partial melting of spinel peridotite: constraints from partitioning studies. *Earth and Planetary Science Letters* **117**, 379–391.

Behrendt, J. C. (1999). Crustal and lithospheric structure of the West Antarctic Rift System from geophysical investigations—a review. *Global and Planetary Change* **23(1–4)**, 25–44.

Behrendt, J. C., LeMasurier, W. E., Cooper, A. K., Tessensohn, F., Tréhu, A. & Damaske, D. (1991). Geophysical Studies of the West Antarctic Rift System. *Tectonics* **10(6)**, 1257–1273.

Berlo, K. & Turner, S. (2010). ($^{210}Pb/^{226}Ra$) disequilibria in volcanic rocks. *Earth and Planetary Science Letters* **296(3–4)**, 155–164, doi:10.1016/j.epsl.2010.05.023.

Blundy, J. & Wood, B. (2003). Mineral–melt partitioning of uranium, thorium and their daughters. In: Bourdon, B., Henderson, G. M., Lundstrom, C. C. & Turner, S. P. (eds) *Uranium Series Geochemistry. Mineralogical Society of America and Geochemical Society, Reviews in Mineralogy and Geochemistry* **52**, 59–123.

Bourdon, B. & Sims, K. W. W. (2003). U-series constraints on intraplate magmatism. In: Bourdon, B., Henderson, G. M., Lundstrom, C. C. & Turner, S. P. (eds) *Uranium Series Geochemistry. Mineralogical Society of America and Geochemical Society, Reviews in Mineralogy and Geochemistry* **52**, 215–253.

Caldwell, D. & Kyle, P. R. (1994). Mineralogy and geochemistry of ejecta erupted from Mount Erebus, Antarctica between 1972 and 1986. In: Kyle, P. R. (ed.) *Volcanological and Environmental Studies of Mount Erebus, Antarctica. American Geophysical Union Antarctica Research Series* **66**, 147–162.

Calkins, J. A., Oppenheimer, C. & Kyle, P. R. (2008). Ground-based thermal imaging of lava lakes at Mount Erebus Volcano, Antarctica in December 2004. *Journal of Volcanology and Geothermal Research* **177**, 695–704.

Charlier, B. L. A. & Zellmer, G. F. (2000). Some remarks on U–Th mineral ages from igneous rocks with prolonged crystallisation histories. *Earth and Planetary Science Letters* **183**, 457–469.

Cheng, H., Edwards, R. L., Hoff, J., Gallup, C. D., Richards, D. A. & Asmerom, Y. (2000). The half-lives of uranium-234 and thorium-230. *Chemical Geology* **169**, 17–33.

Choi, M. S., Francois, R., Sims, K. W. W., Bacon, M. P., Legger-Brown, S., Fleer, A. P., Ball, L. A., Schneider, D. & Pichat, S. (2001). Rapid determination of ^{230}Th and ^{231}Pa in seawater by Inductively coupled plasma mass spectrometry. *Marine Chemistry* **76**, 99–112.

Condomines, M., Sigmarsson, O. & Gauthier, P. J. (2010). A simple model of ^{222}Rn accumulation leading to ^{210}Pb excesses in volcanic rocks. *Earth and Planetary Science Letters* **293(3–4)**, 331.

Cooper, A. K., Davey, F. J. & Behrendt, J. C. (1987). Seismic stratigraphy and structure of the Victoria Land basin, western Ross Sea, Antarctica. In: Cooper, A. K. & Davey, F. J. (eds) *The Antarctic Continental Margin: Geology and Geophysics of the Western Ross Sea*. Houston, TX: Circum-Pacific Council for Energy and Resources, pp. 27–65.

Cooper, K. M. (2009). Comment on 'On the recent bimodal magmatic processes and their rates in the Torfajokull–Veidivotn area, Iceland' by G. F. Zellmer, K. H. Rubin, K. Gronvold and Z. Jurado-Chichay Discussion. *Earth and Planetary Science Letters* **281(1–2)**, 110–114, doi:10.1016/j.epsl.2009.02.007.

Cooper, K. M. & Reid, M. R. (2003). Re-examination of crystal ages in recent Mount St. *Helens lavas: implications for magma reservoir processes*. Earth and Planetary Science Letters **213**, 149–167.

Cooper, K. M., Reid, M. R., Murrell, M. T. & Clague, D. A. (2001). Crystal and magma residence at Kilauea Volcano, Hawaii: $^{230}Th–^{226}Ra$ dating of the 1955 East Rift eruption. *Earth and Planetary Science Letters* **184**, 703–718.

Cooper, K. M., Goldstein, S. J., Sims, K. W.W. & Murrell, M. T. (2003). Uranium-series chronology of Gorda Ridge volcanism: new evidence from the 1996 eruption. *Earth and Planetary Science Letters* **206**, 459–475.

Dawson, J. & Hinton, R. (2003). Trace-element content and partitioning in calcite, dolomite, and apatite in carbonate, Phalaborwa, South Africa. *Mineralogical Magazine* **67(5)**, 921–930.

DePaolo, D. J. (1981). Trace element and isotopic effects of combined wallrock assimilation and fractional crystallization. *Earth and Planetary Science Letters* **53(2)**, 189–202.

Dulaiova, H., Sims, K. W. W., Charette, M. A., Prytulak, J. & Blusztajn, J. S. (2012). A new method for the determination of low-level actinium-227 in geological samples. *Journal of Radioanalytical and Nuclear Chemistry* (in press).

Dulaiova, H., Kim, G., Burnett, W. C. & Horwitz, E. P. (2001). Separation and analysis of Am and Pu from large soil and sediment samples. *Radioactivity and Radiochemistry* **12**, 4–15.

Dunbar, N. W., Cashman, K. V. & Dupre, R. (1994). Crystallization processes of anorthoclase phenocrysts in the Mount Erebus magmatic system: Evidence from crystal composition, crystal size distributions and volatile contents of melt inclusions. In: Kyle, P. R. (ed.) *Volcanological and Environmental Studies of Mount Erebus*, Antarctica. Antarct. Res. Ser., vol. 66. AGU, Washington, D.C., pp. 129–146.

Elkins, L., Gaetani, G. A. & Sims, K. W. W. (2008). Partitioning of U and Th during garnet pyroxenite melting: constraints on sources

of alkaline ocean island basalts. *Earth and Planetary Science Letters* **265**, 270–286, doi:10.1016/j.epsl.2007.10.034.

Elliott, T. (1997). Fractionation of U and Th during mantle melting: a reprise. *Chemical Geology* **139**, 165–183.

Esser, R. P., Kyle, P. R. & McIntosh, W. C. (2004). $^{40}Ar/^{39}Ar$ dating of the eruptive history of Mount Erebus, Antarctica: Volcano evolution. *Bulletin of Volcanology* **66**, 671–686.

Fabbrizio, A., Schmidt, M. W., Guünther, D. & Eikenberg, J. (2009). Experimental determination of Ra mineral/melt partitioning for feldspars and ^{226}Ra-disequilibrium crystallization ages of plagioclase and alkali-feldspar. *Earth and Planetary Science Letters* **280**, 137–148.

Finotello, M., Nyblade, A., Julia, J., Wiens, D. & Anandakrishnan, S. (2011). Crustal V_p–V_s ratios and thickness for Ross Island and the Transantarctic Mountain front, Antarctica. *Geophysical Journal International* **185**, 85–92.

Gauthier, P.-M. & Condomines, M. (1999). Pb–Ra radioactive disequilibria in recent lavas and radon degassing; inferences on the magma chamber dynamics at Stromboli and Merapi volcanoes. *Earth and Planetary Science Letters* **172**, 111–126.

Gauthier, P.-J., Le Cloarec, M.-F. & Condomines, M. (2000). Degassing processes at Stromboli volcano inferred from short-lived disequilibria (^{210}Pb–^{210}Bi–^{210}Po) in volcanic gases. *Journal of Volcanology and Geothermal Research* **102(1)**, 1–19.

Giggenbach, W., Kyle, P. & Lyon, G. (1973). Present volcanic activity on Mt. Erebus, Ross Island, Antarctica. *Geology* **1**, 135–156.

Gill, J., Williams, R. & Bruland, K. (1985). Eruption of basalt and andesite lava degasses ^{222}Rn and ^{210}Po. *Geophysical Research Letters* **12**, 17–20.

Harpel, C. J., Kyle, P. R., Caldwell, D. A., McIntosh, W. C. & Esser, R. P. (2004). $^{40}Ar/^{39}Ar$ dating of the eruptive history of Mount Erebus, Antarctica: summit flows and caldera collapse. *Bulletin of Volcanology* **66**, 687–702.

Harpel, C. J., Kyle, P. R. & Dunbar, N. W. (2008). Englacial tephrostratigraphy of Erebus volcano, Antarctica. *Journal of Volcanology and Geothermal Research* **177(3)**, 549–568, doi:10.1016/j.jvolgeores.2008.06.001.

Hawkesworth, C., George, R., Turner, S. & Zellmer, G. (2004). Timescales of magmatic processes. *Earth and Planetary Science Letters* **218(1–2)**, 1–16, doi:10.1016/S0012-821X(03)00634-4.

Holden, N. E. (1990). Total half-lives for selected nuclides. *Pure and Applied Chemistry* **62**, 941–958.

Hoffmann, D. L., Prytulak, J., Richards, D. A. *et al.* (2007). Procedures for accurate U and Th isotope measurements by high precision MC-ICPMS. *International Journal of Mass Spectrometry* **264**, 97–109.

Horwitz, E. P., McAlister, D. R., Bond, A. H. & Barrans, R. E. (2005). Novel extraction chromatographic resins based on tetraalkyldiglycolamides: Characterization and potential applications. *Solvent Extraction Ion Exchange* **23**, 219.

Jaffey, A. H., Flynn, K. F., Glendenin, L. E., Bentley, W. C. & Essling, A. M. (1971). Precision measurement of half-lives and specific activities of ^{235}U and ^{238}U. *Physical Reviews C* **4**, 1889–1906.

Jochum, K. P., Nohl, U., Herwig, K., Lammel, E., Stoll, B. & Hofmann, A. W. (2005). GeoReM: a new geochemical database for reference materials and isotopic standards. *Geostandards and Geoanalytical Research* **29(3)**, 333–338.

Kayzar, T. M., Cooper, K. M. & Reagan, M. K. (2009). Gas transport model for the magmatic system at Mount Pinatubo, Philippines: Insights from ($^{210}Pb/^{226}Ra$). *Journal of Volcanology and Geothermal Research* **181(1–2)**, 124–140, doi:10.1016/j.jvolgeores.2009.01.006.

Kelly, P. J., Dunbar, N. W., Kyle, P. R. & McIntosh, W. C. (2008*a*). Refinement of the late Quaternary geologic history of Erebus volcano, Antarctica using $^{40}Ar/^{39}Ar$ and ^{36}Cl age determinations. *Journal of Volcanology and Geothermal Research* **177**, 569–577.

Kelly, P. J., Kyle, P. R., Dunbar, N. W. & Sims, K. W. W. (2008*b*). Geochemistry and mineralogy of the phonolite lava lake, Erebus volcano, Antarctica: 1972–2004 and comparison with older lavas. *Journal of Volcanology and Geothermal Research* **177**, 589–605.

Kyle, P. R. (1977). Mineralogy and glass chemistry of recent volcanic ejecta from Mt Erebus, Ross Island, Antarctica. *New Zealand Journal of Geology and Geophysics* **20**, 1123–1146.

Kyle, P. R. (1981). Evolution of a basanite phonolite sequence, Hut Point Peninsula, Antarctica Evidence from Dry Valley Drilling Project Drillholes 1, 2 and 3. *Journal of Petrology* **22**, 451–500.

Kyle, P. (1986). Volcanic activity of Mount Erebus, 1984–1986. *Antarctica Journal of the United States* **XXI**, 7–8.

Kyle, P. R. (1990*a*). McMurdo Volcanic Group–Western Ross Embayment: introduction. In: LeMasurier, W., Thomson, J., Baker, P., Kyle, P., Rowley, P., Smellie, J. & Verwoerd, W. (eds) *Volcanoes of the Antarctic Plate and Southern Oceans. American Geophysical Union, Antarctic Research Series* **48**, 18–25.

Kyle, P. R. (1990*b*). Erebus Volcanic Province. In: LeMasurier, W., Thomson, J., Baker, P., Kyle, P., Rowley, P., Smellie, J. & Verwoerd, W. (eds) *Volcanoes of the Antarctic Plate and Southern Oceans. American Geophysical Union, Antarctic Research Series* **48**, 81–88.

Kyle, P. R. & Cole, J. W. (1974). Structural control of volcanism in the McMurdo Volcanic Group, Antarctica. *Bulletin of Volcanology* **38**, 16–25.

Kyle, P., Dibble, R., Giggenbach, W. & Keys, J. (1982). Volcanic activity associated with the anorthoclase phonolite lava lake, Mt. Erebus, Antarctica. In: Craddock, C. (ed.) *Antarctic Geosciences*. Madison, WI: University of Wisconsin Press, pp. 735–745.

Kyle, P. R., Moore, J. A. & Thirlwall, M. F. (1992). Petrologic evolution of anorthoclase phonolite lavas at Mount Erebus, Ross Island, Antarctica. *Journal of Petrology* **33**, 849–875.

Lambert, G., Bristeau, P. & Polian, G. (1976). Emission and enrichments of radon daughters from Etna volcano magma. *Geophysical Research Letters* **3**, 724–726.

Landwehr, D., Blundy, J., Chamorro-Perez, E., Hill, E. & Wood, B. (2001). U-series disequilibria generated by partial melting of spinel lherzolite. *Earth and Planetary Science Letters* **188**, 329–348.

Larsen, L. M. (1979). Distribution of REE and other trace-elements between phenocrysts and peralkaline undersaturated magmas, exemplified by rocks from the Gardar Igneous Province, South Greenland. *Lithos* **12(4)**, 303–315, doi:10.1016/0024-4937(79)90022-7.

LaTourrette, T. Z., Kennedy, A. K. & Wasserburg, G. J. (1993). U–Th fractionation by garnet—evidence for a deep source and rapid rise by oceanic basalts. *Science* **261**, 739–742.

Layne, G. D. & Sims, K. W. (2000). Secondary ion mass spectrometry for the measurement of $^{232}Th/^{230}Th$ in volcanic rocks. *International Journal of Mass Spectrometry* **203(1–3)**, 187–198.

Le Roux, L. J. & Glendenin, L. E. (1963). Half-life of ^{232}Th. *Proceedings of the National Meeting on Nuclear Energy* **83.**

Lofgren, G. (1980). Experimental studies on the dynamic crystallization of silicate melts. In: Hargrave, R. B. (ed.) *Physics of Magmatic Processes*. Princeton, NJ: Princeton University Press, pp. 487–543.

Lundstrom, C. C., Gill, J., Williams, Q. & Perfit, M. R. (1995). Mantle melting and basalt extraction by equilibrium porous flow. *Science* **270**, 1958–1961.

Martin, P., Hancock, G. J., Paulka, S. & Akber, R. A. (1995). Determination of ^{227}Ac by alpha-particle spectrometry. *Applied Radiation Isotopes* **46(10)**, 1065–1070.

McKenzie, D. (1985). ^{230}Th–^{238}U disequilibrium and the melting processes beneath ridge axes. *Earth and Planetary Science Letters* **72**, 149–157.

Miller, S. A., Burnett, D. S., Asimow, P. D., Phinney, D. L. & Hutcheon, I. D. (2007). Experimental study of radium partitioning between anorthite and melt at 1 atm. *American Mineralogist* **92**, 1535–1538.

O'Hara, M. J. & Mathews, R. E. (1981). Geochemical evolution in an advancing, periodically replenished, periodically tapped, continuously fractionated magma chamber. *Journal of the Geological Society, London* **138**, 237–277.

Oppenheimer, C. & Kyle, P. R. (2008). Probing the magma plumbing of Erebus volcano, Antarctica, by open-path FTIR spectroscopy of gas emissions. *Journal of Volcanology and Geothermal Research* **177**, 743–754.

Oppenheimer, C., Lomakina, A. S., Kyle, P. R., Kingsbury, N. G. & Boichu, M. (2009). Pulsatory magma supply to a phonolite lava lake. *Earth and Planetary Science Letters* **284**, 392–398.

Oppenheimer, C., Moretti, R., Kyle, P., Eschenbacher, A., Lowenstern, J. & Hervig, R. (2011). Mantle to surface degassing of alkalic magmas at Erebus volcano, Antarctica. *Earth and Planetary Science Letters* **306(3–4)**, 261–271.

Pichat, S., Sims, K. W. W., François, R., McManus, J. F., Brown-Legger, S. & Albarède, F. (2004). Lower export production during glacial periods in the equatorial Pacific as derived from (^{231}Pa/^{230}Th) measurements in deep-sea sediments. *Paleoceanography* **19**, PA 4023.

Prowatke, S. & Klemme, S. (2006). Trace element partitioning between apatite and silicate melts. *Geochimica et Cosmochimica Acta* **70**, 4513–4527.

Prytulak, J. & Elliott, T. (2009). Determining melt productivity of mantle sources from ^{238}U–^{230}Th and ^{235}U–^{231}Pa disequilibria; an example from Pico Island, Azores. *Geochimica et Cosmochimica Acta* **73**, 2103–2122.

Prytulak, J., Elliott, T., Hoffmann, D. L. & Coath, C. D. (2008). Assessment of USGS BCR-2 as a reference material for silicate rock U–Pa disequilibrium measurements. *Geostandards and Geoanalytical Research* **32**, 55–63.

Pyle, D., Ivanovich, M. & Sparks, R. S. J. (1998). Magma–cumulate mixing identified by U–Th disequilibrium dating. *Nature* **331**, 157–159.

Reagan, M. K., Volpe, A. M. & Cashman, K. V. (1992). ^{238}U- and ^{232}Th-series chronology of phonolite fractionation at Mt Erebus, Antarctica. *Geochimica et Cosmochimica Acta* **56**, 1401–1407.

Reagan, M. K., Sims, K. W. W., Enrich, J., Thomas, R. B., Cheng, H., Edwards, R. L., Layne, G. D. & Ball, L. A. (2003). Old rhyolite progeny from young mafic parents in North American continental arcs. *Journal of Petrology* **44(9)**, 1703–1726.

Reagan, M. K., Tepley, F. J., Gill, J. B., Wortel, M. & Garrison, J. (2006). Timescales of degassing and crystallization implied by ^{210}Po–^{210}Pb–^{226}Ra disequilibria for andesitic lavas erupted from Arenal volcano. *Journal of Volcanology and Geothermal Research* **157**, 135–146, doi:10.1616/j.jvolgeores.2006.03.044.

Reagan, M. K., Turner, S., Legg, M. K., Sims, K. W. W. & Hards, V. L. (2008). ^{238}U and ^{232}Th decay series constraints on the timescales of crystal fractionation to produce the phonolite erupted in 2004 near Tristan da Cunha, South Atlantic. *Geochimica et Cosmochimica Acta* **72(17)**, 4367–4378.

Robert, J., Miranda, C. F. & Muxart, R. (1969). Mesure de la période du protactinium-231 par microcalorimétrie. *Radiochimica Acta* **11**, 104–108.

Rogers, N. W., Evans, P. J., Blake, S., Scott, S. C. & Hawkesworth, C. J. (2004). Rates and timescales of fractional crystallization from ^{238}U–^{230}Th–^{226}Ra disequilibria in trachyte lavas from Longonot Volcano, Kenya. *Journal of Petrology* **45**, 1747–1776.

Rubin, K. H. (1997). Degassing of metals and metalloids from erupting seamount and mid-ocean ridge volcanoes: observations and predictions. *Geochimica et Cosmochimica Acta* **61**, 3525–3542.

Rubin, K. H. & Zellmer, G. F. (2009). Reply to Comment on 'On the recent bimodal magmatic processes and their rates in the Torfajökull–Veidivötn area, Iceland' by K. *M. Cooper*. Earth and Planetary Science Letters **281**, 115–123, doi:10.1016/j.epsl.2009.02.008.

Rubin, K. H., Macdougall, J. D. & Perfit, M. R. (1994). ^{210}Po–^{210}Pb dating of recent volcanic eruptions on the sea floor. *Nature* **368**, 841–844.

Rubin, K. H., I., v.d.Z., Smith, M. C. & Bergmanis, E. C. (2005). Minimum speed limit for ocean ridge magmatism from ^{210}Pb–^{226}Ra–^{230}Th disequilibria. *Nature* **437**, 22.

Sato, J. (2003). Natural radionuclides in volcanic activity. *Applied Radiation and Isotopes* **58**, 393–399.

Sato, K. & Sato, J. (1977). Estimation of gas-releasing efficiency of erupting magma from ^{226}Ra–^{222}Rn disequilibrium. *Nature* **226**, 439–440.

Sato, K., Kaneoka, I. & Sato, J. (1980). Rare-gas releasing experiments and Rn degassing from erupting magma. *Geochemical Journal* **14**, 91–94.

Seaman, S. J., Dyar, M. D., Marinkovic, N. & Dunbar, N. (2006). An FTIR study of hydrogen in anorthoclase and associated melt inclusions. *American Mineralogist* **91(1)**, 12–20.

Shimizu, N. & Hart, S. R. (1982*a*). Applications of the ion microprobe to geochemistry and cosmochemistry. *Annual Review of Earth and Planetary Sciences* **10**, 483–526.

Shimizu, N. & Hart, S. R. (1982*b*). Isotope fractionation in secondary ion mass spectrometry. *Journal of Applied Physics* **53**, 1303–1311.

Sims, K. W. W. & Gauthier, P. J. (2007). Characterizing degassing and magma recharge from measurement of short-lived U-series isotopes in volcanic gases and lavas. *Geochimica et Cosmochimica Acta* **71(15)**, A941–A941.

Sims, K. W. W. & Hart, S. R. (2006). Comparison of Th, Sr, Nd and Pb isotopes in oceanic basalts: implications for mantle heterogeneity and magma genesis. *Earth and Planetary Science Letters* **245**, 743–761, doi:10.1016/j.epsl.2006.02.030.

Sims, K. W. W., DePaolo, D. J., Murrrell, M. T., Baldridge, W. S., Goldstein, S. J. & Clague, D. (1995). Mechanisms of magma generation beneath Hawaii and mid-ocean ridges: U–Th and Sm–Nd isotopic evidence. *Science* **267**, 508–512, doi:10.1126/science.267.5197.508.

Sims, K. W. W., Murrell, M. T., DePaolo, D. J., Baldridge, W. S., Goldstein, S. J., Clague, D. & Jull, M. (1999). Porosity of the melting zone and variations in the solid mantle upwelling rate beneath Hawaii: Inferences from ^{238}U–^{230}Th–^{226}Ra and ^{235}U–^{231}Pa disequilibria. *Geochimica et Cosmochimica Acta* **63(23)**, 4119–4138, doi:10.1016/S0016-7037(99)00313-0.

Sims, K. W. W., Goldstein, S. J., Blichert-Toft, J. *et al.* (2003). Chemical and isotopic constraints on the generation and transport of melt beneath the East Pacific Rise. *Geochimimica et Cosmochimica Acta*, **66(19)**, 3481–3504, doi:10.1016/S0016-7037(02)00909-2.

Sims, K. W. W., Ackert, R. P., Jr, Ramos, F., Sohn, R. A., Murrell, M. T. & DePaolo, D. J. (2007). Determining eruption ages and erosion rates of Quaternary basaltic volcanism from combined U-series disequilibria and cosmogenic exposure ages. *Geology* **35**, 471–474, doi:10.1130/G23381A.1.

Sims, K. W. W., Blichert-Toft, J., Kyle, P. R., Pichat, S., Bluzstajn, J., Kelly, P. J., Ball, L. A. & Layne, G. D. (2008*a*). A Sr, Nd, Hf, and Pb isotope perspective on the genesis and long-term evolution of alkaline magmas from Erebus volcano, Antarctica. *Journal of Volcanology and Geothermal Research* **177**, 606–618.

Sims, K. W. W., Gill, J., Dossetto, A., Hoffmann, D., Lundstrom, C. C., Williams, R., Ball, L. A., Tollstrup, D., Turner, S. P.,

Prytulak, J., Glessner, J., Standish, J. J. & Elliott, T. (2008*b*). An inter-laboratory assessment of the Th isotopic composition of synthetic and rock standards. *Geostandards and Analytical Research* **32(1)**, 65–91.

Sims, K. W. W., Hart, S. R., Reagan, M. K., Blusztajn, J., Staudigel, H., Sohn, R. A., Layne, G. D., Ball, L. A. & Andrews, J. (2008*c*). ^{238}U–^{230}Th–^{226}Ra–^{210}Pb–^{210}Po, ^{232}Th–^{228}Ra and ^{235}U–^{231}Pa constraints on the ages and petrogenesis of Vailulu and Malumalu Lavas, Samoa. *Geochemistry, Geophysics, Geosystems* **9**, Q04003, doi:10.1029/2007GC001651.

Snyder, D., Widom, E., Pietruszka, A. J. & Carlson, R. W. (2004). The role of open-system processes in the development of silicic magma chambers: a chemical and isotopic investigation of the Fogo A trachyte aeposit, São Miguel, Azores. *Journal of Petrology* **45**, 723–738.

Snyder, D. C., Widom, E., Pietruszka, A. J., Carlson, R. W. & Schmincke, H.-U. (2007). Timescales of formation of zoned magma chambers: U-series disequilibria in Fogo A and 1563 A.D. trachyte deposits, São Miguel, Azores. *Chemical Geology* **239**, 138–155.

Spiegelman, M. & Elliott, T. (1993). Consequences of melt transport for uranium series disequilibria. *Earth and Planetary Science Letters* **118**, 1–20.

Stracke, A., Bourdon, B. & McKenzie, D. (2006). Melt extraction in the Earth's mantle: Constraints from U–Th–Pa–Ra studies in oceanic basalts. *Earth and Planetary Science Letters* **244(1–2)**, 97–112.

Sumner, C. (2007). Residence time estimates and controls on crystallization patterns for anorthoclase phenocrysts in phonolite magma, Erebus Volcano, Antarctica. MS thesis. Socorro: New Mexico Institute of Mining and Technology **278**, p.

Sun, S.-S. & Hanson, G. N. (1975). Origin of Ross Island basanitoids and limitations upon the heterogeneity of mantle sources for alkali basalts and nephelinites. *Contributions to Mineralogy and Petrology* **54**, 139–55.

Sweeney, D., Kyle, P. R. & Oppenheimer, C. (2008). Sulfur dioxide emissions and degassing behavior of Erebus volcano, Antarctica. *Journal of Volcanology and Geothermal Research* **177**, 725–733.

Tuli, J. K. (2000). *Nuclear wallet cards*, . Upton, NY: Brookhaven National Laboratory **114**, p.

Turner, S. P., George, R. M. M., Jerram, D. A., Carpenter, N. & Hawkesworth, C. J. (2003). Case studies of plagioclase growth and residence times in island arc lavas from Tonga and the Lesser Antilles, and a model to reconcile discordant age information. *Earth and Planetary Science Letters* **214**, 279–294.

Turner, S. P., Black, S. & Berlo, K. (2004). ^{210}Pb–^{226}Ra and ^{226}Ra–^{230}Th systematics in young arc lavas: Implications for magma degassing and ascent rates. *Earth and Planetary Science Letters* **227**, 1–16.

Vazquez, J. A. & Reid, M. R. (2002). Time scales of magma storage and differentiation of voluminous high-silica rhyolites at Yellowstone caldera, Wyoming. *Contributions to Mineralogy and Petrology* **144(3)**, 274–285, doi:10.1007/s00410-002-0400-7.

Volpe, A. M. & Hammond, P. E. (1991). ^{238}U–^{230}Th–^{226}Ra disequilibria in young Mount St. Helens rocks: time constraint for magma formation and crystallization. *Earth and Planetary Science Letters* **107**, 475–486.

Waters, C. L., Sims, K. W. W., Perfit, M. R., Blichert-Toft, J. & Blusztajn, J. (2011). Linking volcanic resurfacing and magmatic cycling: evidence from isotopically enriched basalts at 9–10°N East Pacific Rise. *Journal of Petrology* **52(3)**, 565–602, doi:10.1093/petrology/egq091.

Williams, R. W. & Gill, J. B. (1989). Effects of partial melting on the uranium decay series. *Geochimica et Cosmochimica Acta* **53**, 1607–1619.

Zellmer, G. F. & Clavero, J. (2006). Using trace element correlation patterns to decipher a sanidine crystal growth chronology: an example from Taapaca volcano, Central Andes. *Journal of Volcanology and Geothermal Research* **156**, 291–301.

Zellmer, G. F., Rubin, K. H., Grönvold, K. & Jurado-Chichay, Z. (2008). On the recent bimodal magmatic processes and their rates in the Torfajökull–Veidivötn area, Iceland. *Earth and Planetary Science Letters* **269**, 387–397, doi:10.1016/j.epsl.2008.02.026.

Zreda-Gostynska, G., Kyle, P. R., Finnegan, D. & Prestbo, K. M. (1997). Volcanic gas emissions from Mount Erebus and their impact on the Antarctic environment. *Journal of Geophysical Research* **102(B7)**, 15039–15055.

APPENDIX A

ANALYTICAL METHODS FOR MEASUREMENT OF ^{227}AC AND ^{228}TH

^{227}Ac

The dissolved rock samples were spiked using ~0·5 d.p.m. g^{-1} of rock of NIST certified ^{229}Th/^{225}Ac tracer in equilibrium. Samples were re-heated to allow for better tracer equilibration. Actinides from the sample solution were preconcentrated via lead sulfate co-precipitation (Martin *et al.*, 1995), which was then dissolved in 20 ml of 4 M HCl. This solution was loaded on a commercially available extraction chromatographic column containing N,N,N',N'-tetra-n-octyldiglycolamide [DGA column manufactured by Eichrom (Horwitz *et al.*, 2005)]. In 4 M HCl, the actinides are well retained on the DGA column whereas common ions and alkaline earth elements have no affinity and pass through the column without retention. Several column volumes of 3 M HNO_3 then rinse the leftover alkaline earth elements and iron from the column. In the next step we eluted actinium with 2 M HCl, which recovers Ac but leaves Th and other actinides retained on the DGA. The actinium fraction was prepared for alpha spectrometric measurement via cerium fluoride micro-precipitation (Dulaiova *et al.*, 2001). The samples were counted immediately for ^{225}Ac, from which we determined chemical recoveries, and then again in about 60 days after the ingrowth of ^{227}Ac daughters ^{227}Th + ^{223}Ra. The ^{225}Ac chemical recoveries were 67 ± 11% ($n = 23$). The minimum detectable activities (MDA) of ^{227}Ac using alpha spectrometry were 0·001 d.p.m. per sample using an acquisition time of 1 week.

^{228}Th

The (^{228}Th/^{232}Th) value for an anorthoclase erupted in December 2005 was determined by alpha spectrometry in April 2008. Five grams of sample were digested in a mixture of concentrated HF and HNO_3. After evaporation to dryness, the sample was completely dissolved in about

Table A1: Individual in situ Ba and Th concentrations in anorthoclase megacrysts (AN) and their melt inclusions (MI) and for selected pyroxene (PX) and adhering glass spots (GL) measured by SIMS (IMS-3f Cameca) at WHOI

Name		Type	Location	Ba (ppm)	Th (ppm)
ER84-01					
ER84-01	3	MI	core	453·3	37·37
ER84-01	7	MI	core	572·4	31·02
ER84-01	8	MI	core	654·6	34·68
ER84-01	14	MI	rim	402·2	26·81
ER84-01	18a	MI	core	471·4	34·26
ER84-01	18b	MI	core	434·7	32·51
ER84-01	22a	MI	core	442·1	25·19
Av.				490	31·7
1σ SD				90	4·4
ER84-01	11	GL			37·16
ER84-01	16a	GL		520·4	27·95
ER84-01	16b	GL		478·0	25·84
ER84-01	1	AN	core	2583·2	0·092
ER84-01	4	AN	core	2239·3	
ER84-01	5	AN	core	2399·7	0·110
ER84-01	6	AN	core/rim	2255·8	0·092
ER84-01	9	AN	core/rim	2374·7	
ER84-01	12	AN	core	2742·0	
ER84-01	15a	AN	rim	2234·8	
ER84-01	15b	AN	rim	2093·0	0·141
ER84-01	19a	AN	core	1935·7	0·100
ER84-01	19b	AN	core	1775·4	0·131
ER84-01	20a	AN	core	1835·8	0·141
ER84-01	20b	AN	core		0·012
ER84-01	23b	AN	rim	1952·9	0·092
ER84-01	26b	AN	rim	1984·5	0·093
Av.				2185	0·10
1σ SD				291	0·04
ER84-01	2	PX	core	2·9	0·194
ER84-01	17-1	PX	core	2·5	0·097
ER84-01	17-2	PX	core	1·4	0·012
ER84-04					
ER84-04	2	MI	rim	552·5	31·27
ER84-04	3	MI	core/rim	510·8	24·72
ER84-04	6	MI	core	588·5	
ER84-04	8	MI	core	517·6	30·45
ER84-04	10	MI	core	546·9	25·70
ER84-04	12	MI	rim	576·0	
Av.				549	28·0
1σ SD				31	3·3
ER84-04	1	GL		499·7	24·44
ER84-04	14	GL		529·7	22·08
ER84-04	4	AN	core/rim	2288·2	0·02
ER84-04	5	AN	rim	2250·1	0·00
ER84-04	7	AN	core	2327·7	0·03
ER84-04	9	AN	core	2213·2	0·05
ER84-04	13	AN	rim	2313·7	0·03
Av.				2279	0·026
1σ SD				47	0·021
ER88-01					
ER88-01	1	MI	core	413·7	26·11
ER88-01	2	MI	core	409·4	26·08
ER88-01	5	MI	core	413·2	26·98
ER88-01	6	MI	core	424·1	25·09
ER88-01	8	MI	core	399·0	23·47
ER88-01	10	MI	core	419·8	25·39
ER88-01	12	MI	core	398·7	22·63
ER88-01	16	MI	core/rim	392·2	22·72
ER88-01	17	MI	rim	388·9	21·56
ER88-01	18	MI	rim	416·1	22·12
ER88-01	20	MI	rim	450·4	
ER88-01	27	MI	core/rim	389·2	29·17
Av.				409·6	24·66
1σ SD				17·7	2·36
ER88-01	21	GL		389·3	22·24
ER88-01	24	GL		386·1	21·99
ER88-01	3	AN	core	1883	0·192
ER88-01	4	AN	core	2051	0·012
ER88-01	7	AN	core	2031	0·215
ER88-01	9b	AN	core	1829	0·012
ER88-01	11	AN	core	1781	0·153
ER88-01	13	AN	core	1829	0·109
ER88-01	14b	AN	core/rim	1846	0·282
ER88-01	15	AN	core/rim	1881	
ER88-01	19	AN	rim	1893	0·125
ER88-01	23	AN	rim	1793	0·114
ER88-01	25	AN	rim	1942	0·123
ER88-01	26	AN	rim	1769	0·082
ER88-01	28	AN	rim	1840	
ER88-01	29	AN	rim		0·156
ER88-01	30	AN	core/rim		0·150
Av.				1840	0·13
1σ SD				54	0·07

(continued)

Table A1: Continued

125 ml of 1 N HCl with 5 ml of saturated boric acid. A few drops of an $FeCl_3$ solution were added to this solution, followed by concentrated NH_3OH, until iron oxy-hydroxides ceased precipitating. The Th-bearing iron precipitate was then separated from the supernate by centrifuging. The supernate was discarded and the precipitate was dissolved in 2 ml concentrated HNO_3, dried, re-dissolved in 7·5 N HNO_3 and run through an anion exchange column

charged with nitric acid. The Th was washed off with 6 N HCl and dried. The Th was then dissolved in 5 ml of a 2 M ammonium chloride solution adjusted to pH = 2·1 using HCl plus 1 ml of a saturated ammonium oxalate solution (pH = 2·0), and electroplated on a stainless steel disk using 2 amps of current over 20 min. The plated sample was alpha-counted for 12 days. Data reduction included subtracting background counts, tails of higher energy peaks into lower energy peaks, and the portion of the ^{224}Ra peak (a short-lived daughter of ^{228}Th) that is within the energy range counted for ^{228}Th. The total adjustments to the raw counts were 2–4% for ^{230}Th and ^{232}Th and 17% for ^{228}Th.

APPENDIX B

MODEL CALCULATIONS FOR CONTINUOUSLY RECHARGED OPEN-SYSTEM MODEL

Our open-system model algorithm is the following. It should be noted that recharge (step 5) is omitted for closed-system crystallization modeling.

For each iteration:

(1) one increment of anorthoclase by volume is added onto the pre-existing crystals using a mass-balance equation, and the composition of the entire crystal mass is recalculated. The degree of fractionation for each step is chosen so the model approximates measured compositions in 10 000 steps.
(2) The composition of the melt is then recalculated for the growth of the entire fractionating assemblage.
(3) ^{210}Po is degassed from the magma 1·3% per day to best fit the model to the data. ^{222}Rn is presumed to be in equilibrium with ^{226}Ra based on the equilibrium (^{210}Pb/^{226}Ra) measured in both the anorthoclase crystals and glass.
(4) The activities of all radioactive nuclides in both the bulk anorthoclase and remaining melt are readjusted for radioactive ingrowth and decay. These calculations include any intermediate daughters of the decay series (e.g. ^{228}Ra, where the measured nuclide is actually ^{228}Th).
(5) New magma is added proportionally to the amount of crystallization based on a constant rate of recharge/crystallization [the 'r' value of DePaolo (1981)].

This is iterated for 10 000 steps.